UNIVERSITY OF PAVIA
FACULTY OF ENGINEERING

UNIVERSITY SCHOOL OF ADVANCED
STUDIES - IUSS PAVIA

Does the vertical component of ground motion matter for Seismic Risk Assessment? Two illustrative cases

A Thesis Submitted in Partial Fulfilment of the Requirements
for the Degree of Master of Science (Laurea Magistrale) in

Civil Engineering for the Mitigation of Risk from Natural Hazards
Reduction of Seismic Risk (ROSE) curriculum

by

Georgios Triantafyllou

Supervisors: Prof. Paolo Bazzurro Prof. Dimitrios Vamvatsikos

February, 2021 a.a. 2019-2020

ABSTRACT

This thesis attempts to investigate some cases where the vertical component of ground motion might be important for regular Seismic Risk assessment studies. For this purpose, two separate studies are addressed. The first part of the study is dedicated to the influence of the vertical component on the P-Δ effects, due to the variation of gravity load during an earthquake. For this purpose, a single degree of freedom (SDOF) model is built in OpenSees from the pushover analysis of a 2D multiple degree of freedom (MDOF) model. Multiple stripe analysis (MSA) is performed for both the SDOF and the MDOF model with, and without the inclusion of the vertical component of ground motion. It is found that, by including the vertical component, the lateral response of the structure is not significantly affected, except for a few cases. The second part of this study addresses the vulnerability of non-structural components such as suspended ceilings when the vertical component of ground motion is included in the analysis. For this purpose, a 2D model of a steel moment resisting frame, capable of predicting vertical floor accelerations at various locations of the floor level is created in OpenSees. Plus, with the use of some performance criteria of the ceilings against the vertical component found in literature, fragility functions of the ceilings are created against the vertical floor accelerations and a framework for the loss estimation of ceilings subjected to both horizontal and vertical floor accelerations is developed. The findings of this study suggest that the inclusion of the vertical component of ground motion is very important for the non-structural loss of the ceilings, and its neglection may lead to a severe underestimation of the total loss of a structure.

ACKNOWLEDGEMENTS

TABLE OF CONTENTS

LIST OF FIGURES

LIST OF TABLES

1. INTRODUCTION

The impact of the vertical component of ground motion on the structural seismic response and loss estimates is not investigated as much as that of the horizontal component. Several studies has shown that for very specific cases, the vertical component might be important for the structural response of a structure [Eltahawy et al (2017); Ryan & Dao (2016); Korzec (2016); Carydis et al (2012)]. However, it is difficult to find a study that pushes the research towards taking into account the vertical component of ground motion in seismic risk assessment. This study examines two cases, where the vertical component is well-known to be important for the response but it is not quantified yet whether or not it is important for regular seismic risk assessment studies.

Several authors have discussed the importance of the vertical component of ground motion on the seismic response of a structure. Bazzurro et al (2020) discuss the extension of the Conditional Spectrum (CS) method to select a set of hazard consistent 3-component records for the risk assessment of a liquid storage tank. Tanks are prone to uplifting due to horizontal excitation, a behavior that can be exacerbated by the vertical component of the ground motion. Different record selection approaches were tested with and without consideration of the vertical component, as well as with and without vertical ground motion hazard consistency. It was found that there is a non-negligible dependence of the tank response to the effects of the vertical component, which should be included when estimationg the response of such structures. Neglecting it typically results in an underestimation of the maximum uplift demand by 20%. In addition, it is recommended to incorporate the hazard consistency of the vertical component in the record selection, because it does have an impact on the tank response.

Kohrangi et al (2020) discuss the correlation of Spectral acceleration values of vertical and horizontal ground motion pairs. Correlation coefficient estimates are presented between a number of ground motion intensity measures (IMs), extracted from the NGA-West2 database, with focus on the correlation of vertical-vertical and vertical-horizontal ground motion components. The IMs considered include Spectral Accelerations with periods from 0.01s to 10s, Peak Ground Acceleration, Peak Ground Velociy, and Significant Duration (for 5-75% and 5-95% definitions). To facilitate their use, parametric equations are also fitted to correlation models. Finally, the dependence of the obtained correlation coefficients to magnitude, distance and V_{S30} is evaluated.

Kwong et al (2020) discuss the extension of the CS to include the vertical component of ground motion, and present an approach to select multicomponent ground motions that are hazard consistent with respect to all three components of ground motion. Korzec (2016) discuss the effect of the vertical acceleration on the stability assessment of seismically loaded earth dams. Fayaz & Zareian (2019) assess the effects of the verrtical component of ground motion on steel structures and evaluates the current seismic design provions of ASCE 7 (2016) provides on the basis of a structural reliability outlook. It is concluded that current seismic load combinations in ASCE 7 are inadequate to account for the effects of the vertical component of near-fault ground motions. Liberatore et al (2019) discuss the effects of coseismic vertical ground motion on masonry constructions damage during the 2016 Amatrice-Norcia earthquakes. Hariri-Ardebili & Saouma, (2016) explores the seismic fragility curves for gravity dams with or without the vertical component of ground motion.

Di Michele et al (2020) discuss the effects of the vertical component of ground motion on the in-plane response of masonry walls. It is found that for records characterized by low source-to-site distance and high moment magnitudes, the vertical component can generate tensile forces in the masonry piers, especially where the gravity loads are small, and in these cases, fluctuations in the axial load strongly affect the flexural and shear capacity of the masonry piers. Ryan & Dao (2016) discuss the influence of the vertical ground shaking on horizontal response of seismically isolated buildings with friction bearings. The study focuses on a horizontal-vertical coupling effect observed in a full-scale shake table experiment of a 5-story moment frame building isolated with triple pendulum bearings. A significant increase or amplification of the horizontal floor accelerations was observed during the three-dimensional shaking compared to the horizontal only XY shaking. The vertical component of ground acceleration is shown to introduce a high-frequency component into the base shear that can excite higher modes of the base isolated structure. Kale & Akkar (2020) discuss a new formulation for a code-based vertical design spectrum.

The first part of the current study is dedicated to the effect of the vertical component of ground motion on the lateral response of a structure through the P-Δ effects. It is well known, that the vertical component creates a variation of gravity loads during the earthquake shaking, and this variation might increase the P-Δ effects on a structure, and thus might increase the values of the Engineering Demand Parameters (EDP's). This was investigated by performing Multiple Stripe Analysis (MSA), using several bi-directional ground motion records, and applying them to both a Single Degree of Freedom (SDOF) model and a multiple degree of freedom (MDOF) model. The scope is to identify whether the inclusion of the vertical component generate a lateral response of a typical building that is statistical significantly different than that obtained using only the horizontal components of motion.

The second part of the study is dedicated to the performance of non-structural components such as suspended ceilings when the vertical component of ground motion is included in the analysis. For this purpose, a two-dimensional (2D) model is created capable of estimating vertical floor accelerations at various locations of the floor. Then, some performance metrics, which were established after a large-scale experiment, are used to develop fragilities of the ceilings against the vertical component, and a ceiling loss assessment is performed using the horizontal and vertical floor accelerations as EDP's.

The structure of the thesis is organized as follows. The 2nd chapter discusses the effect of the vertical component on the P-Δ effects. The 3rd chapter adresses the vertical floor acceleration demands on non-structural elements along with the loss estimation of the ceilings. Then Chapter 4 outlines the conclusions.

2. VERTICAL COMPONENT AND P-Δ effects

2.1 OVERVIEW

The scope of this chapter is to investigate the influence of the vertical component of ground motion on the response and stability of a structure when 2nd order effects are included. It is well known that P-Δ effects lead to a stiffness reduction and a rotation of the hysteresis curve, which affects the maximum inter-story drift ratio (IDR) and residual drifts. Herein we focus on the effect of the vertical component to the variation of gravity loads during a Nonlinear Time History Analysis (NLTHA), and thus on the lateral response of the structures. The model used in this study is a Single Degree of Freedom (SDOF) bilinear model. Although such models are rather simplistic compared to Multiple Degree of freedom (MDOF) models and may not capture the real behavior of a structure during an earthquake, their usefulness lies to their simplicity of defining different parameters and tracking the sensitivity of the response to them.

There are a few studies discussing the effect of the vertical component of ground motion on the lateral response of a structure. Zou et al (2018) investigates the influence factors of P-Δ effects, considering the vertical ground motion. That paper discusses the influence of stiffness-to weight ratio, structural damping, and the vertical acceleration response of the structure on the P-Δ effects and concludes that the inclusion of the vertical component of ground motion, affects the displaced shape of an MDOF model. Spears (2004) discusses the parameters influencing structural collapse with an emphasis on vertical ground accelerations. One part of the study performs Incremental Dynamic Analysis (IDA), using bilinear SDOF models representative of low-rise buildings (3-5-9 stories). It shows that the vertical acceleration can affect the ductility demands of a model with negative post-yield stiffness ratio.

Kalkan & Graizer (2007) discussed the effects of multiple components of the ground motion, including the vertical component. In this paper, a governing equation of motion was postulated to compute the response of a SDOF oscillator under a multi-component excitation. This equation includes secondary P-Δ components associated with the combined impacts of tilt and vertical excitation, in addition to the inertia force terms due to the angular and translational accelerations. They propose a multi-component response spectrum which reflects kinematic characteristics of the ground motion that are not identifiable by the conventional spectrum itself, at least for a near-fault region where high

intensity vertical shaking and rotational excitations are likely to occur. They mention that if the direction of the vertical pulses is in-phase with the gravity, then they may reduce the overall stiffness of the system by increasing the contribution of the geometric stiffness term. On the contrary, if the vertical pulses are out of phase with gravity, then they tend to minimize the destabilizing force. They conclude that the vertical component of ground motion leads to enhanced P-Δ effects, and therefore for structures susceptible to high-intensity vertical shaking, multi-component effects should be considered in seismic design, or performance assessment.

Ghaffarzadeh & Nazeri (2015) discussed the effect of the vertical component of ground motion on the horizontal response. A computer program was prepared to perform nonlinear dynamic analysis based on the derived governing equations of motions including the vertical component. They conclude that, the system effective stiffness is a parameter that depends on vertical vibration response, vertical ground motion acceleration, mass and height of structure and that the horizontal displacement increases by considering the horizontal and vertical components of ground motion acting simultaneously.

In the following pages, details about the structural modelling of the SDOF and MDOF case study building are presented. We also provide information about the ground motion records used in this study and the results of the NLTHA with and without the inclusion of the vertical component. Four type of analyses are performed: unidirectional without P-Δ effects, unidirectional with P-Δ effects, bidirectional without P-Δ effects, and bidirectional with P-Δ effects.

2.2 STRUCTURAL MODELLING

A 7-story reinforced concrete moment resisting system building is used as a reference for this study. This is a modern structure build to post-1980 seismic design provisions for high-seismicity regions (site class D). Table 2-1 shows some of the main features of the building. The analyses carried out on both SDOF and MDOF model. The MDOF model was built in a previous study (Kazantzi & Vamvatsikos, 2015), and it was used for running NLTHA including the vertical component of ground motion. The SDOF model was built in the current study based on the pushover response of the MDOF model.

Table 2-1: MDOF structure characteristics

Building ID	No1
No of stories, n_s	7
Height of first story, h_1 (m)	6.91
Height of 2nd and above stories, h_i (m)	3.96
$X = h_1/h_i$	1.74

Total height (m)	30.7
Gravity/Lateral tributary areas	0.17
Tributary mass in each frame per floor (tn)	313
Fundamental period, T_1 (sec)	1.58

The fundamental period, T_1, in the table is the horizontal period coming from 1st order analysis (excluding P-Δ effects). The fundamental period coming from 2nd order analysis is 1.64 seconds.

2.2.1 Equivalent SDOF model description

The schematic view of the SDOF model depicted in Figure 2-1. The model is created in OpenSees(Mckenna, 2011) and is meant to represent the behavior of the 7-storey MDOF structure. The model consists of a pinned rigid bar with a rotational spring at the base, which is simulating the equivalent lateral behavior of the MDOF structure based on the pushover analysis of the MDOF model. The rigid bar and the rotational spring are conceptually, springs in series, so the flexibility of the system is totally represented by the rotational spring, which also defines the lateral strength of the system, since the rigid bar is elastic. A lumped mass is attached at the top of the bar, while a finite-length damper is used for energy dissipation purposes.
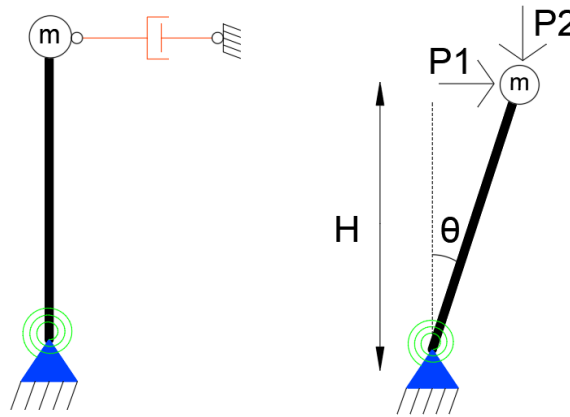
Figure 2-1: Schematic view of the SDOF Model. Left: undeformed shape; Right: deformed shape

For the rigid bar, an *elasticBeamColumn* element was used with high area, *A*, and moment of inertia, *I*, in order to provide high axial and flexural stiffnesses. The gravity load was applied at the top of the bar with a linear time series, and the mass was assigned in both horizontal and vertical direction in order to provide inertial forces coming from the horizontal and

the vertical components of ground motion. The vertical component of ground motion creates a variation of gravity loads during the NLTHA, so the geometric stiffness is also changing. In OpenSees, if one includes P-Δ transformation, the geometric stiffness is updated at each time step.

The lateral stiffness of the model was provided by the rotational spring which was modelled as a *zeroLength* element, with a bilinear law assigned to the *UniaxialMaterial* command in OpenSees. The *Steel01* material was employed for assigning a bilinear law with kinematic hardening. Damping was introduced to the system with a truss member defined with viscous damping material assigned to it rather than stiffness. The specific damping modelling procedure was adopted from (Spears, 2004). Except for the damping coefficient c, the damper has a finite length and area, and its properties are selected after damping ratio convergence in free vibration analysis.

The force-deformation law of the SDOF system is determined from the base shear-roof displacement relationship of a 1-st mode pattern nonlinear pushover analysis of the MDOF structure, without including P-Δ effects. The procedure followed to model the SDOF parameters is based on (Fajfar, 2000). The procedure for defining the SDOF parameters, is presented in Appendix A. The bilinearization of the capacity curve of SDOF was done based on the equal area assumption. The target displacement point in order to apply equal energy assumption (D_m*) is illustrated in Figure 2-2 (D* and F* in the figure refer to the top displacement and Base shear of the SDOF model after they have been reduced from the MDOF respective quantities by means of the Γ factor). The properties of the rotational spring were derived through a moment equilibrium of the rigid bar with respect to the base. The contribution of the gravity load on the moment equilibrium was not taken into account, since the yielding properties of the rotational spring are defined for 1st order analysis, with the P-Δ effects coming automatically in the analysis with the P-Δ transformation in OpenSees.
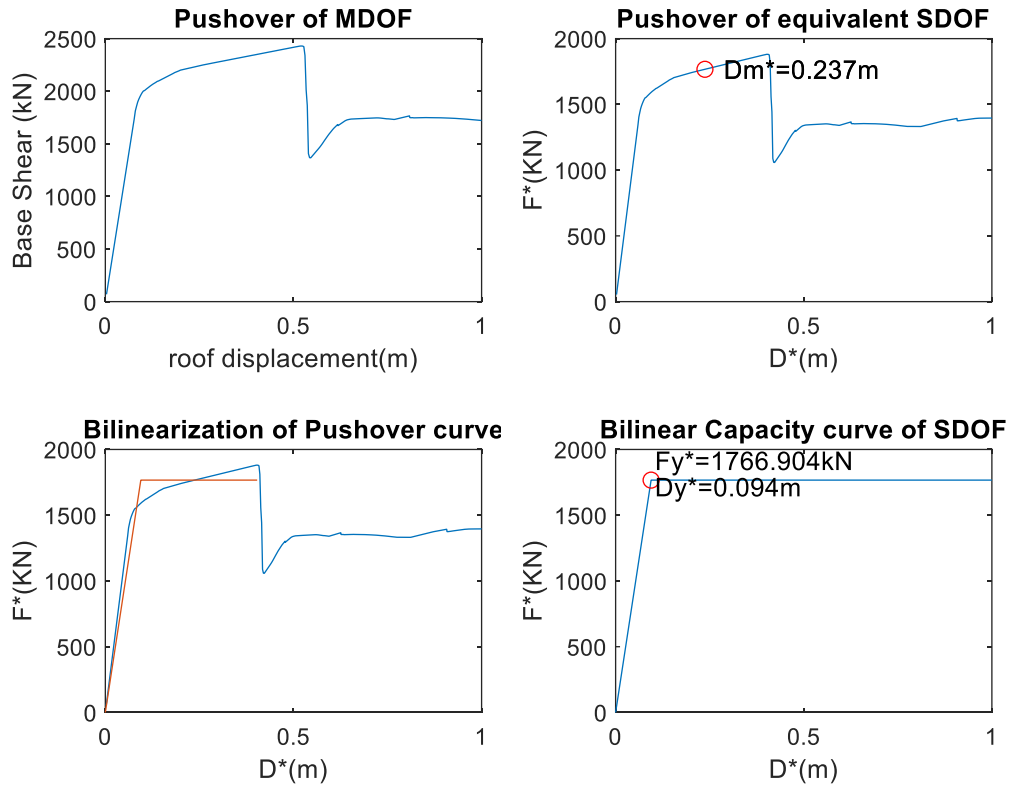
Figure 2-2: Pushover bilinearization

After the definition of the properties of the rotational spring at the base, 1% kinematic hardening was also applied to the SDOF model. A pushover analysis was carried out for the SDOF OpenSees model, with and without 2nd order effects. When including P-Δ effects, the nonlinear branch of the pushover is characterized by negative stiffness, while the yielding force is also smaller (Figure 2-3).
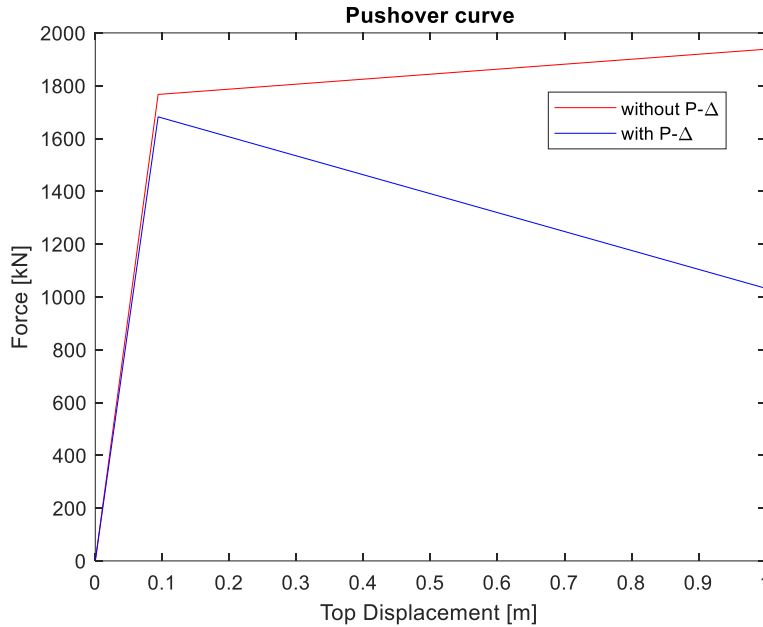
Figure 2-3: Pushover curve of the SDOF model

2.2.2 MDOF model description

The MDOF structure is a Reinforced Concrete building, symmetric in plan. Kazantzi & Vamvatsikos (2015) created a centerline 2D idealization of the specific structure using OpenSees. The behavior of the structural members was modelled with lumped plasticity elements, with the hinge properties modelled with the empirical equations proposed by Panagiotakos & Fardis (2001). The plastic hinge rotational springs have a moment-rotation relationship with a quadrilinear backbone incorporating moderate pinching hysteresis, in-cycle strength and stiffness degradation together with an ultimate fracturing rotation. Geometric nonlinearities in the form of P-Δ effects were considered. In the present study, lumped vertical masses were added in the columns in order to provide inertial forces coming from the vertical component of ground motion.

2.3 GROUND MOTION DATABASE

The bidirectional ground motion records used in this study are derived from Bazzurro et al. (2020). In that specific study, a site of major oil refineries in Elefsina, Greece, is adopted to perform all probabilistic seismic hazard analysis (PSHA) computations. Seismic response analysis of a 3D liquid storage tank was performed using four hazard-consistent variants of record selections, all based on the CS (conditional spectrum) method. In all cases the conditioning scalar IM (intensity measure) in the horizontal plane was the geometric mean

of spectral acceleration from both horizontal components of the ground motion, $Sa_h (T_i)$ at a period of T_i=0.3s. The target spectra for each conditioning IM were based on the mean M-R scenarios obtained from the disaggregation results of PSHA for the selected site. The current study uses the records derived from the record selection case, CS-C_{xyz} (Conditional spectrum - Correlation horizontal & vertical). In this specific record selection case, the conditioning IM was the geometric mean of spectral acceleration of two horizontal components at T_i, and the records were selected and scaled to match the target spectrum of the geomean (horizontal) and vertical components considering the correlation of spectral accelerations. The spectral shapes at both horizontal and vertical components are, therefore, compatible with the hazard. Seventy records are selected for each stripe, and herein we perform Multiple Stripe Analysis for seven stripes with 50, 10, 5, 2, 1.0, 0.6, 0.2 % probability of exceedance in 50 years.
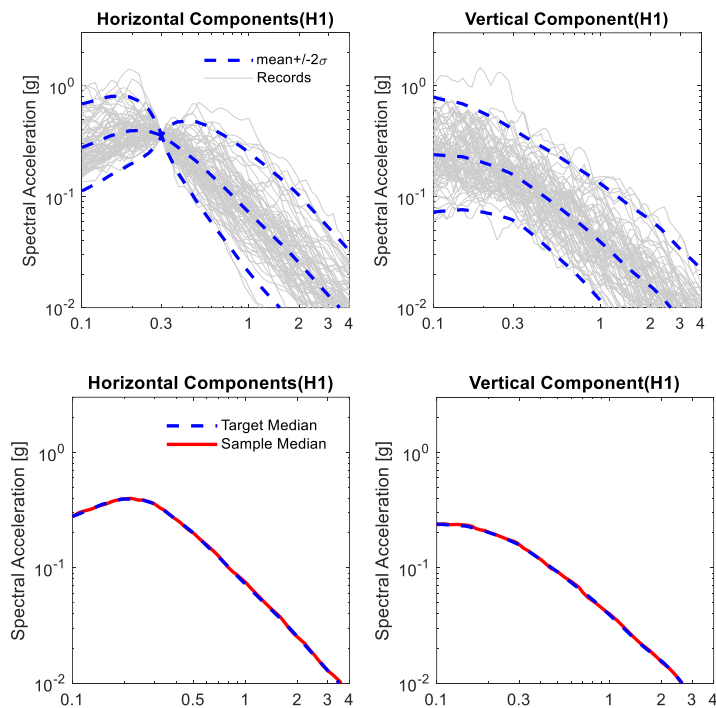
Figure 2-4: Illustration of the CS record set used for the analysis

2.4 RESULTS

Nonlinear dynamic analyses of the SDOF and MDOF models were performed for ground motion records associated with each intensity level. As mentioned earlier, four types of analyses were performed for each ground motion record, including:

(i) bidirectional with P-Δ effects, denoted as HV2ndOrder
(ii) bidirectional without P-Δ effects, denoted as HV1stOrder
(iii) unidirectional with P-Δ effects, denoted as H2ndOrder
(iv) unidirectional without P-Δ effects, denoted as H1stOrder

and the maximum drift caused by each case is recorded. Intuitively, a variation of drifts is expected to be seen in the cases of bi-directional with P-Δ effects (HV2ndOrder) and unidirectional with P-Δ effects (H2ndOrder). This difference would indicate the importance of including the vertical component in the calculation of the response. Conversely, no difference is expected in the drifts caused by the unidirectional without P-Δ effects and bidirectional without P-Δ effects cases.

2.4.1 SDOF results

As expected, Figure 2-5 confirms that the inclusion of the vertical component for 1st order analysis makes no difference in the specific SDOF model. The vertical component would influence the response of structures composed by fiber elements, and thus the variation of gravity load would affect the moment-rotation response of a section, but the purpose of this research is to examine the effect solely on the P-Δ effects. The maximum drift values of the SDOF system from the cases of unidirectional analysis (no vertical component), with and without P-Δ effects is presented in Figure 2-6. The inclusion of P-Δ effects is more pronounced on the higher IM levels, where the nonlinearity of the structure becomes more significant. The purpose of Figure 2-7 is to examine the importance of including the vertical component in the 2nd order analysis. The vertical component has no statistical importance on the maximum drift values and only few outlier values are observed. The same trend is observed in Figure 2-8 and Figure 2-9, where the maximum drift at each stripe and the ductility demand of the rotational spring are plotted respectively.

One possible explanation for this trend is the fact that the vertical component and the horizontal component input motions are not in phase. Moreover, the horizontal period is different than the vertical period, which in this case is close to zero, since the bar is axially rigid. Having input ground motions which are not in phase and two transfer functions far separated from each other reduces the probability of interactions between the two components.

EDP=maximum Roofdrift
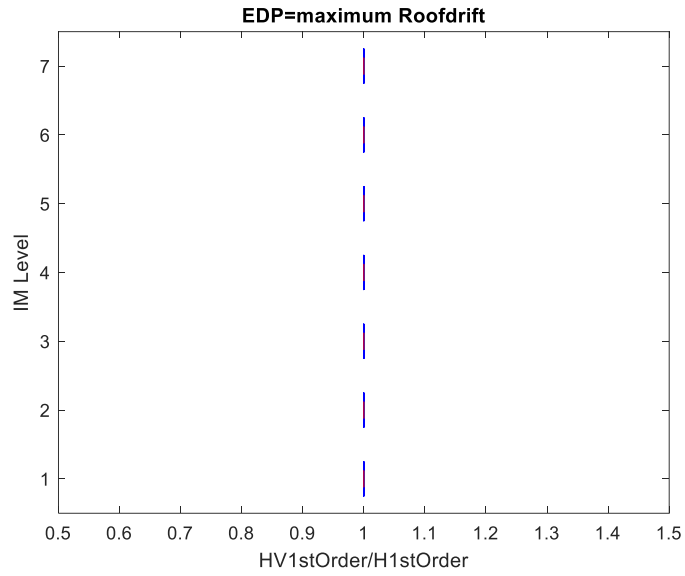
Figure 2-5: Boxplot comparison of maximum roofdrift between bidirectional 1st order and unidirectional first order analysis

EDP=maximum Roofdrift

Figure 2-6: Boxplot comparison of maximum roofdrift between unidirectional 2nd order and unidirectional 1st order analysis

Figure 2-7: Boxplot comparison of maximum roofdrift between bidirectional 2nd order and unidirectional 2nd order analysis
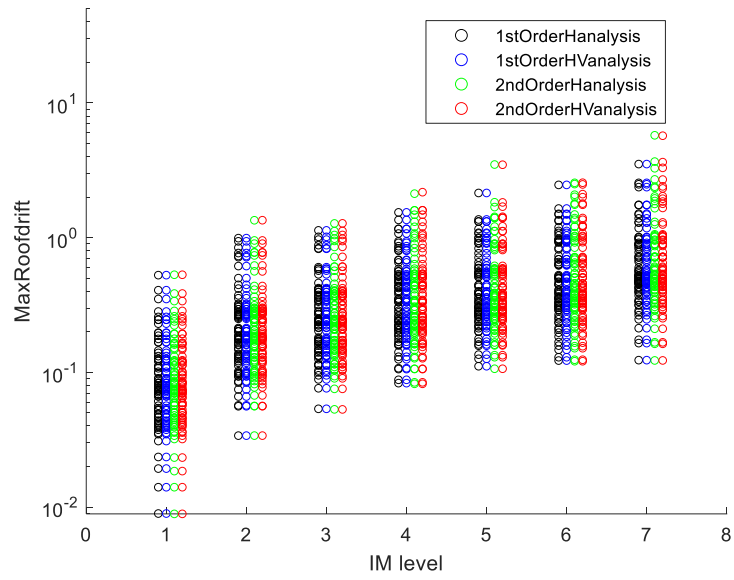
Figure 2-8: Maximum roof drift comparison for various IM levels
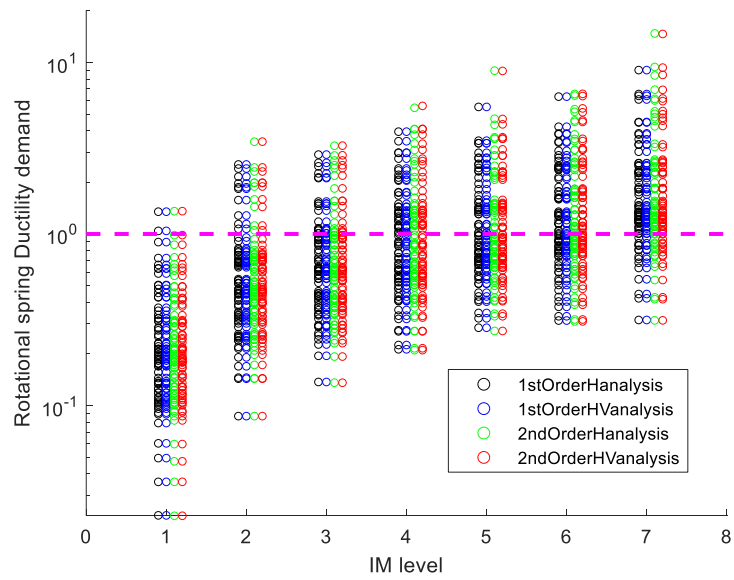
Figure 2-9: Rotational spring ductility demand for various IM levels

Why, contrary to intuition, is there so little difference? To answer this question, we focus on an outlier point, where the inclusion of the vertical component is important for the lateral response of the SDOF model. As illustrated in Figure 2-11, the inclusion of the vertical component affects both the maximum roofdrift and the residual drift. For this ground motion record, the vertical component seems to reduce P-Δ effects. The hysteresis curves for the four types of analyses are also plotted in Figure 2-12 and Figure 2-13 , where it is evident that the inclusion of the vertical component changes the hysteresis response of the SDOF.

At this point an additional scaling factor ($2*SF_v$) is applied to the vertical component of ground motion, in order to better illustrate the H-V interaction. By increasing the scaling factor of the vertical component, the 2nd order response comes very close to the 1st order response, so the P-Δ effects are even further reduced, as it is seen in Figure 2-14 and Figure 2-15.

An additional scaling factor ($5*SF_v$) is further applied to the vertical component of ground motion in order to illustrate an interesting aspect of the interaction of the two components. By looking to Figure 2-16 it seems that by further increasing the scaling factor of the vertical component, the damage accumulates in the other direction. This is attributed to the amplification of some vertical pulses that increase the P-Δ effects in the other loading direction. One could argue that the vertical component might add or remove "strength" from the horizontal pulses, depending on the timing and the sign of the vertical component. By looking at Figure 2-17, it can be seen that the vertical component alternates the hysteresis path, with the damage, being accumulated in the other direction. Given that the scaling factor of the vertical component is further increased, then these pulses that increase the P-Δ effects on that direction will lead to a further increase on the maximum drift and residual drift.

The question that arises is: what makes this ground motion so special regarding the interaction of the horizontal and vertical component so that the drifts computed with and without the application of the vertical component are so different? The significant duration was estimated for both components in terms of Arias Intensity (AI), with the significant duration D_{5-95}=20.8 seconds for the horizontal component, and D_{5-95}=25.5 seconds for the vertical component (Figure 2-18). Furthermore, both components are rich in low frequencies, (Figure 2-19) and the vertical component changes the gravity loads for some amount of time in a specific pattern (either increasing or decreasing the gravity loads), without changing sign immediately, as it would happen if the vertical component had only high frequency content.
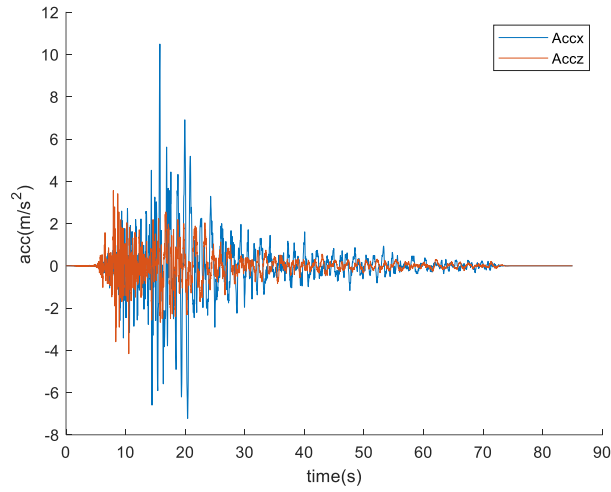
Figure 2-10: Bidirectional ground acceleration time history-IM6/Chi Chi 1999, Sequence number=3467, NGA-West
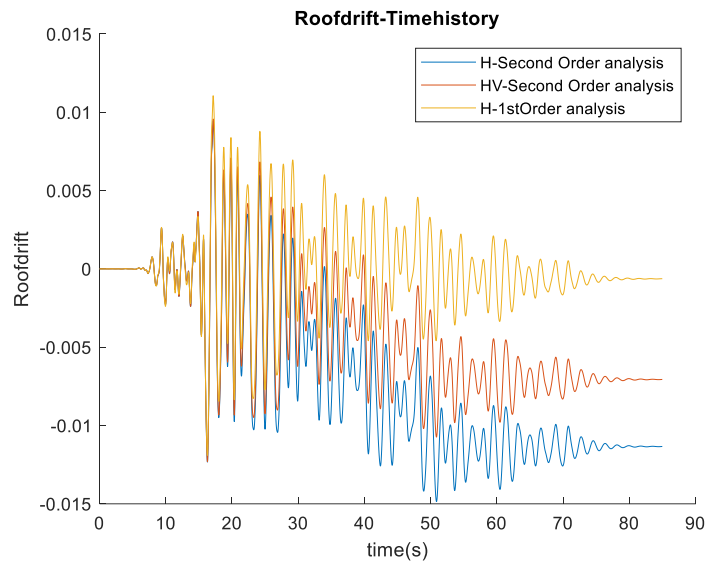
Figure 2-11: Roofdrift time histories for 3 different types of analysis
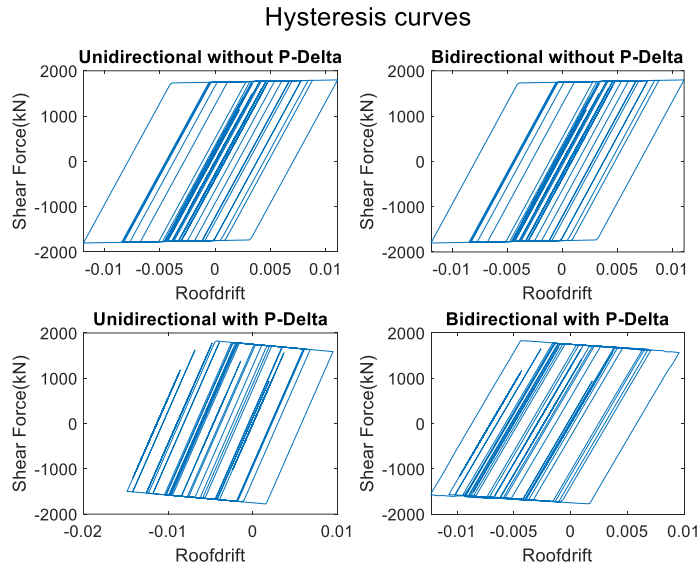
Figure 2-12: Hysteresis plots for different types of analysis
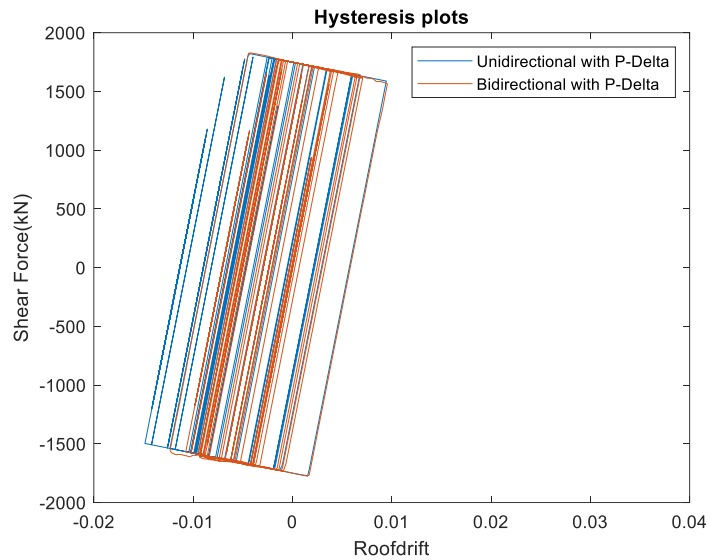
Figure 2-13: Comparison of 2nd order hysteresis plots with and without vertical component
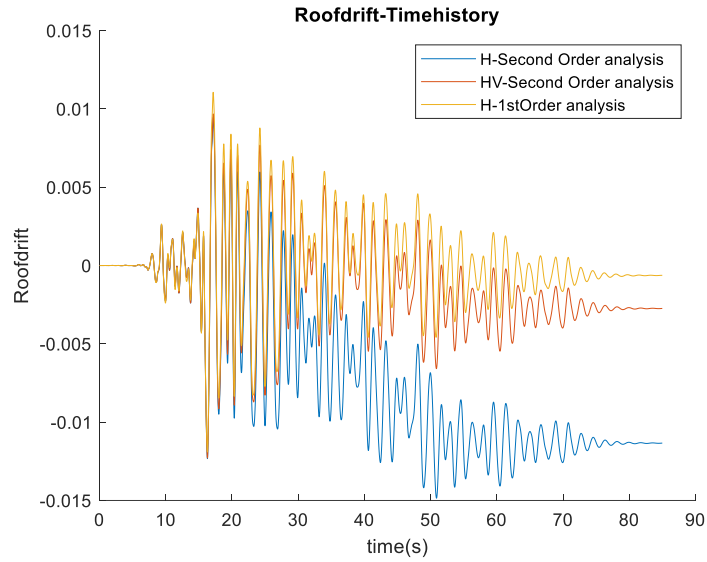
Figure 2-14: Roofdrift time history for 3 different types of analysis-2*SFv
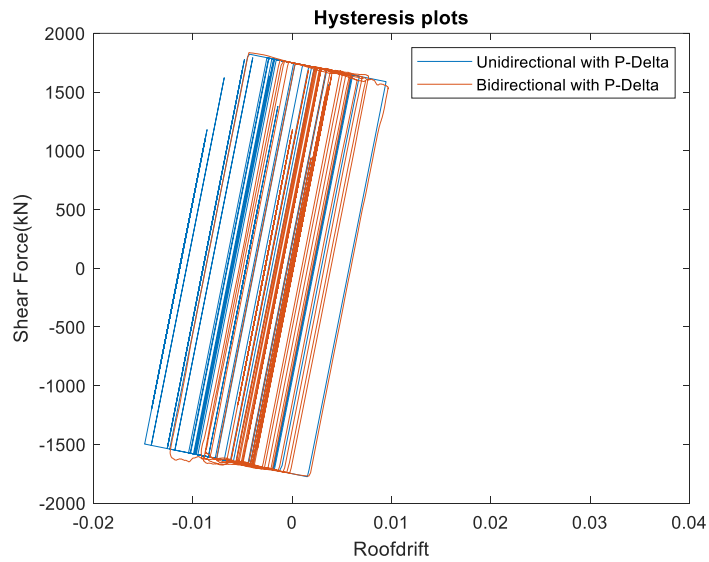
Figure 2-15: Comparison of 2nd order hysteresis plots with and without vertical component-2*SFv
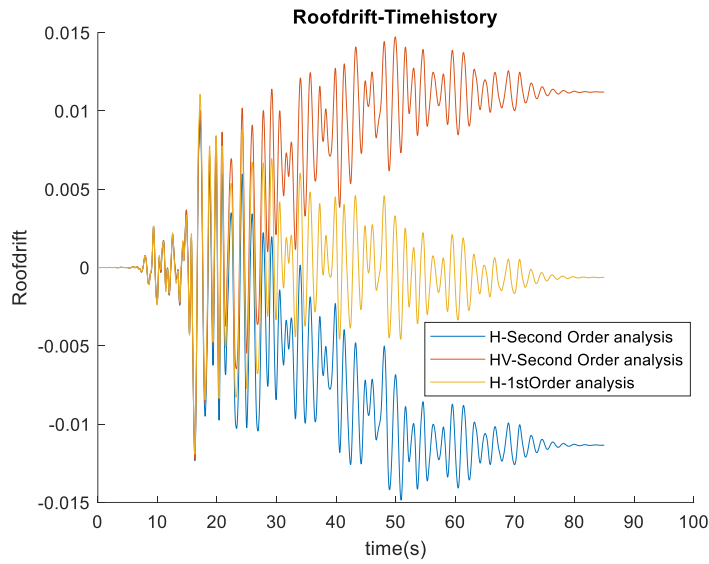
Figure 2-16: Roofdrift time history for 3 different types of analysis-5*SFv
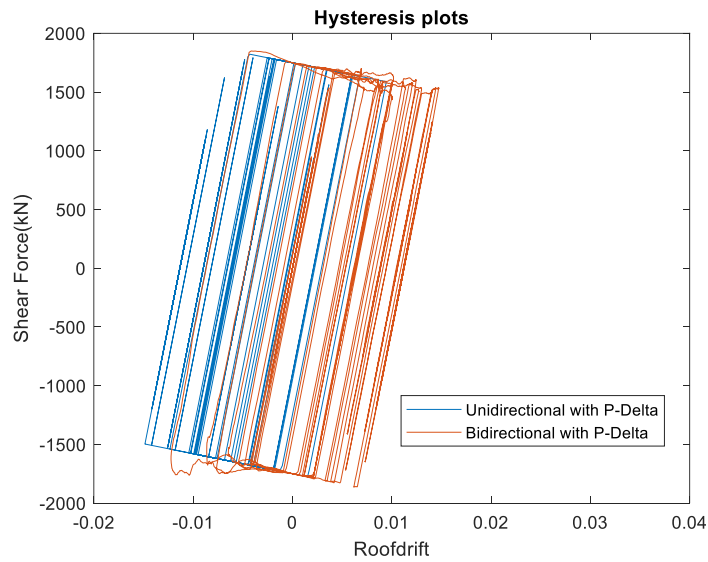
Figure 2-17: Comparison of 2nd order hysteresis plots with and without vertical component-5*SFv
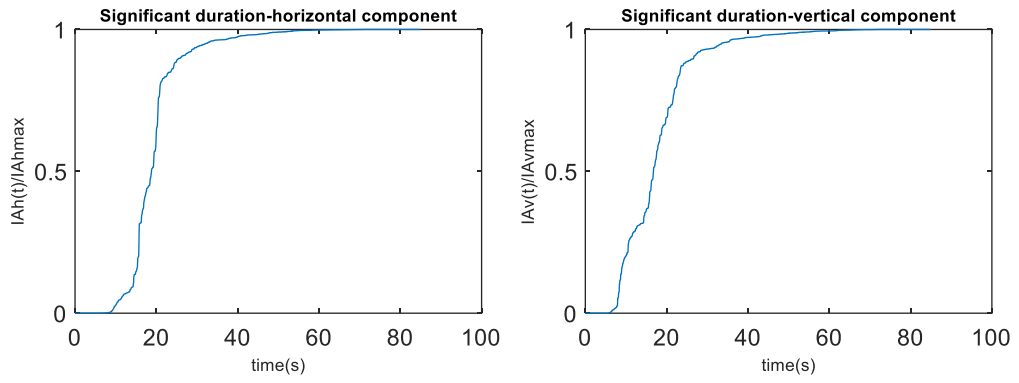
Figure 2-18: Significant duration for horizontal and vertical components
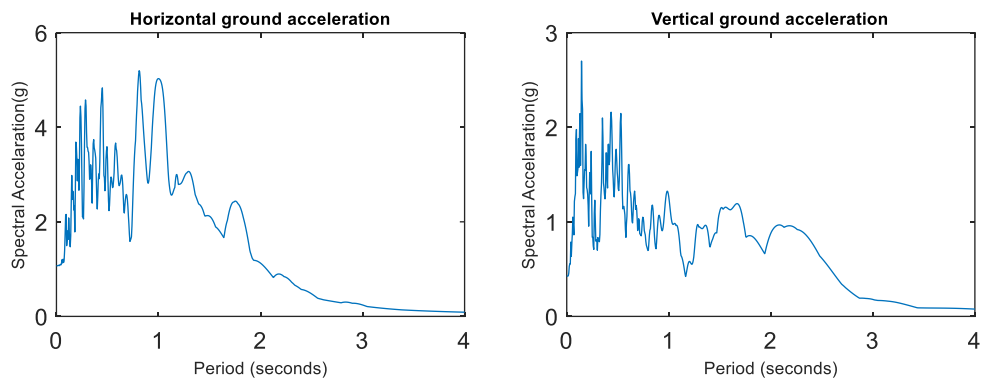
Figure 2-19: Ground acceleration Spectra

2.4.2 MDOF results

The MDOF structure was subjected to the same set of ground motions. All the drift outputs of the SDOF model are turned to MDOF quantities, by multiplying them by the Γ factor. The maximum roofdrift of the MDOF structure is compared with the maximum drift of the SDOF model through a boxplot (Figure 2-20). By looking at this boxplot, it can be seen that the median is very close to 1 across all IM levels, which means that overall, the response of the structure is well captured by the SDOF model. At higher IM levels, the nonlinear effects are more pronounced, the response becomes more complex, and the inter-quartile distance becomes wider. Higher mode effects, especially at high IM levels, influence the response, an influence that is of course lost in the SDOF model that can only capture the 1st mode response. Moreover, in the MDOF model the plastic hinges are modelled with lumped plasticity elements, which experience pinching behavior, and this makes the response more complex compared to that computed via the SDOF model where all response is lumped at the base rotational spring that follows a bilinear kinematic hardening law. Furthermore, the response is also sensitive to the bilinearization of the pushover curve of the equivalent SDOF system, since this slightly changes the period of the SDOF system compared to that of the MDOF model.

Figure 2-21 depicts the importance of the P-Δ effects on the lateral response of the MDOF structure. As the intensity of the ground motion increases, the drift differences become more important since the material and geometric nonlinearity are more pronounced at higher IM levels. Again, as shown in Figure 2-22, the inclusion of the vertical component does not change much the maximum roofdrift of the MDOF model. However, more outliers are present compared to the SDOF model case. This difference may be attributed to the fact that P-Δ effects are more severe in the MDOF model, along with the fact that the MDOF model has some flexibility in the vertical direction, unlike the SDOF system which was rigid. This flexibility may lead to a spectral amplification of the vertical ground acceleration and, thus, to a higher variation of the gravity loads.
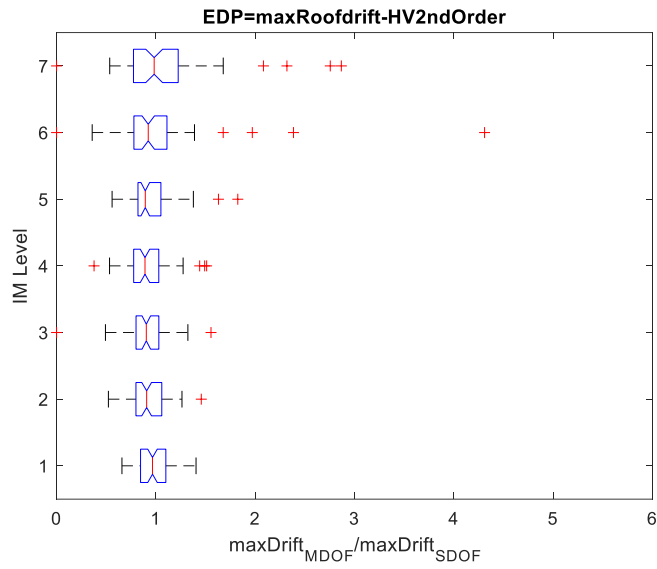
Figure 2-20: Boxplot comparison of the maximum roofdrifts of the MDOF structure with the maximum drifts of the SDOF model.
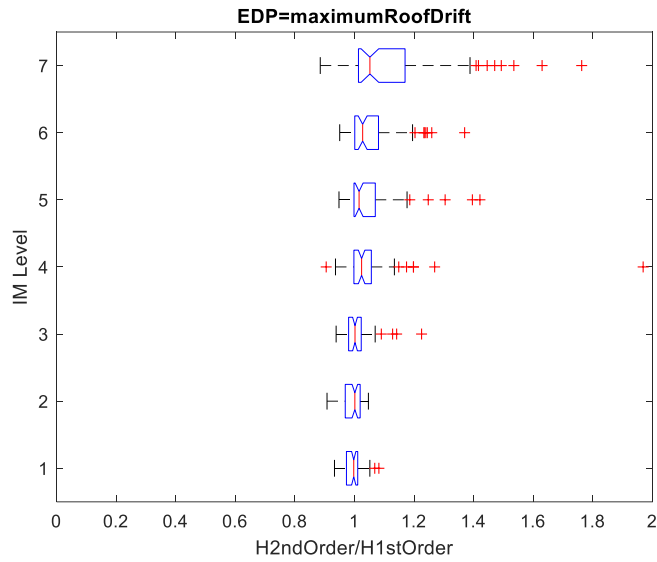
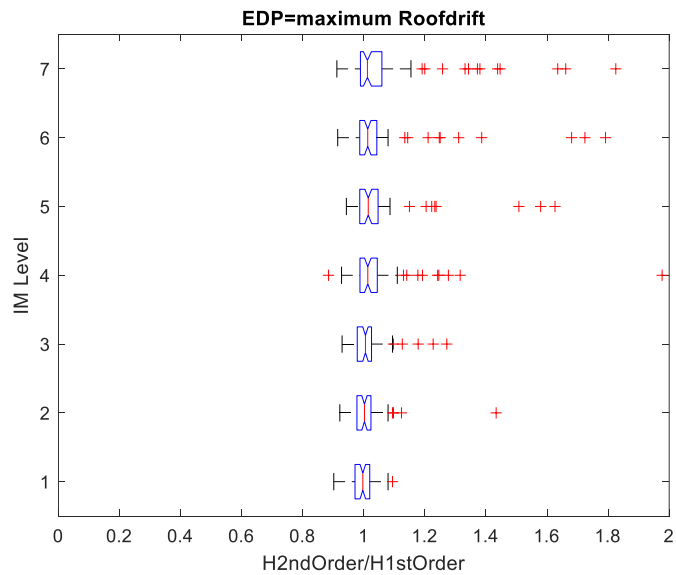**Figure 2-21: Boxplot comparison of maximum roofdrifts from the unidirectional 2nd order and unidirectional 1st order analyses of the MDOF structure**
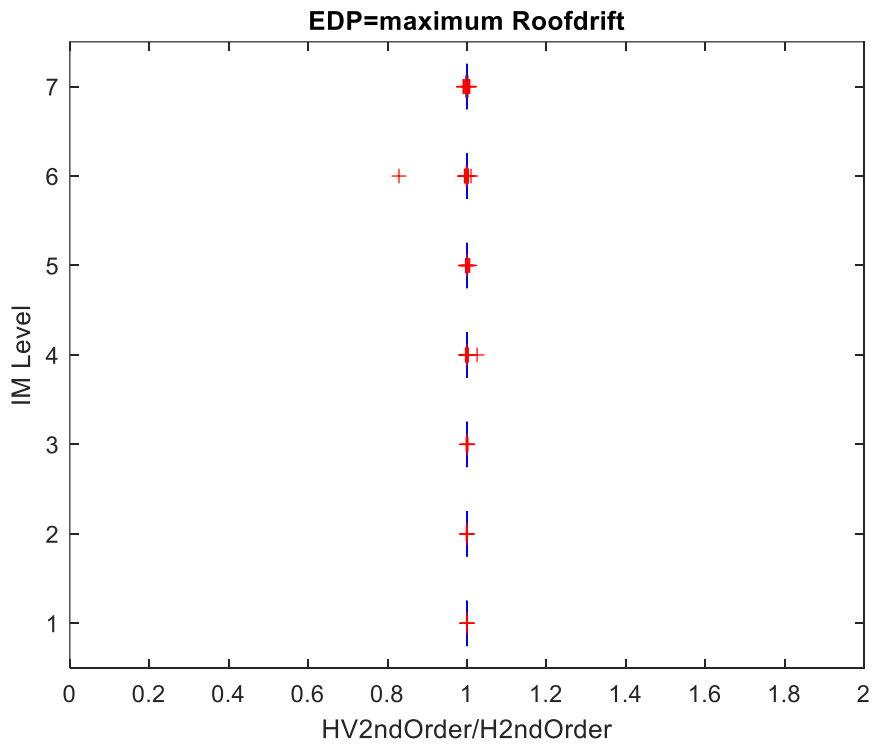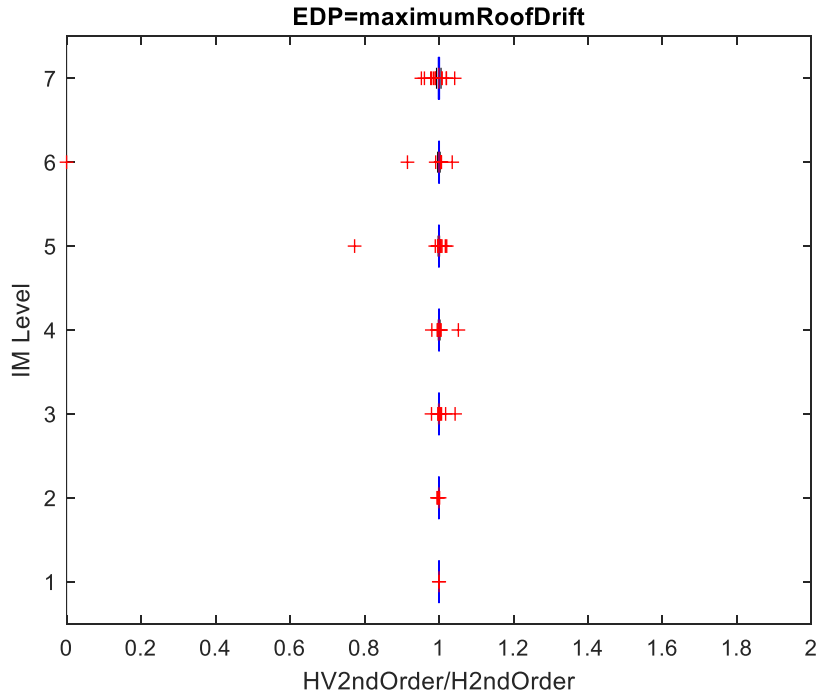
Figure 2-22: Boxplot comparison of maximum roofdrifts from the bidirectional 2nd order and unidirectional 2nd order analyses of the MDOF structure.

2.5 CONCLUSIONS

By performing MSA on both the SDOF and the MDOF models of this structure, it was found that there is little impact of the vertical component on its lateral response even when the P-Δ effects are accounted for. This happens mainly because the input vertical ground motion and the horizontal ground motion are generally out of phase due to seismological reasons. In addition, the horizontal and vertical periods are far separated from each other. These two aspects make the probability of HV (Horizontal-Vertical) interaction in the response low. These results, however, only apply to this structure. Additional models more prone to P-Δ effects (like structures with significant irregularities, and soft-storey effects) should be tested along with different ground motions to better understand the impact of the vertical component on the dynamic P-Δ effect phenomenon.

3. VERTICAL FLOOR ACCELERATION DEMANDS TO Non-Structural Components

3.1 OVERVIEW

The objective of this chapter is to investigate the floor acceleration demands on non-structural components (NSC) such as suspended ceilings, and estimate damage to them, when the vertical component of ground motion is included in the analysis. For this purpose, a two-dimensional (2D) building model was created, which is capable of estimating floor accelerations, both in horizontal and vertical directions. The first part of this chapter, is dedicated to the development of the 2D model, including the moment resisting frame (MRF) and the gravity system, with the latter being modelled in such a way, to be able to predict the vertical floor accelerations at various locations of the floor level, such as the column-line, along the primary beam, and at the middle of the secondary beams (open-bay estimate). The second part of this chapter is dedicated to the development of a framework for loss estimation of non-structural components sensitive to both horizontal and vertical floor accelerations.

NSCs such as suspended ceilings, fire-sprinkler piping system and electric generators, shall be designed to withstand vertical inertial forces. ASCE 7 provides an equivalent Static Design Force, $F_{pv}=\pm 0.2S_{DS}*W_p$, where S_{DS} is the design earthquake spectral response acceleration at short period, and W_p is the operating weight of the nonstructural component. In that way, the code assumes no amplification by height for the vertical acceleration demand of the nonstructural components.

Few studies recognize the importance of the vertical component of ground motion on the response of NSC sensitive to vertical floor acceleration demands. Moschen et al (2016) addressed the statistical evaluation of vertical peak floor acceleration (PFA$_V$) demands on elastic multistory buildings. The model used in that study is a generic stick model representing the column-line of the steel perimeter moment frame. They found that the median PFA$_V$ demand along the column can be up to four times larger than the vertical peak ground acceleration (PGA$_V$). Assi et al (2017) discuss the horizontal and vertical acceleration amplification at the roof level, and they examine the parameters affecting the vertical acceleration amplification by height, including the building vertical period of

vibration, the number of stories, and the location of the building relative to the causative fault.

Gremer et al (2019) discuss the vertical peak floor acceleration demands at column lines an along the length of beams of elastic moment-resisting steel frames subjected to recorded ground motions. The results of this study indicate that the vertical peak floor accelerations can be amplified up to 5 times compared to the vertical peak ground acceleration, in contrast to horizontal peak floor acceleration, where the amplification is around two times the horizontal peak ground acceleration. The higher amplification factors were found at the center of the girders of the moment-resisting frame. They mention that the story-wise mass distribution has an influence not only on the vertical acceleration demand, but also on the horizontal component of the response, although to a lesser degree. They conclude that it is highly questionable to ignore the amplification of the vertical acceleration along the height of the structure.

Ryan et al (2016), discussed the seismic response of a full-scale 5-story steel moment resisting frame building in base-isolated and fixed-base configurations with an integrated suspended ceiling-partition wall-sprinkler piping system that was tested on the shake table at E-Defense. Horizontal accelerations were constrained by the isolation systems to relatively low levels. This allowed linking the observation of damage to the acceleration-sensitive non-structural components only to the vertical component of input acceleration. Peak vertical accelerations were amplified by an average factor ranging from 3 to 6, on the middle of the floor slab. That study defined vertical floor acceleration values associated with the onset of different damage states.

Wieser (2011) discusses the assessment of floor accelerations in nonlinear finite element models. This study uses 3D finite element models of four steel moment-resisting frames. Incremental Dynamic Analysis is employed to evaluate the floor response of inelastic steel moment frame buildings subjected to all three components of a suite of 21 ground motion records. This study focuses on the influence of structural period, level of ductility of the structure and relative height along the building on the horizontal and vertical floor acceleration response. The horizontal floor acceleration response is shown to decrease with increasing structural period and ductility while varying nonlinearly along the height of the building. The vertical acceleration response was found to be independent of structural period, level of ductility and relative height. Variation in the vertical acceleration response is primarily attributed to the out-of plane flexibility of the floor system. Significant vertical acceleration amplification is only observed away from the column supports.

Herein, we propose a 2D-model capable of estimating vertical floor acceleration demands at several locations of the floor, by including the gravity system beams and columns, which are more flexible compared to those in the moment resisting frames and thus, higher

amplification factors are expected at these locations. Moreover, by using the vertical acceleration metrics established by Ryan et al (2016), we attempt to provide a framework for the loss estimation of a suspended-ceiling system, taking into account both the horizontal and vertical floor acceleration demands. The chapter is organized as follows. First, a section about the structural modelling is presented, then the ground motion database and the probabilistic seismic demand of floor accelerations is addressed, and finally the results of the loss estimation procedure for the ceilings are presented.

3.2 BUILDING DESCRIPTION AND STRUCTURAL MODELLING

The model used for this study is a 2D representation of the LA-9 building. The structure is a 9-storey steel, moment-resisting frame with a single-storey basement. Vamvatsikos & Fragiadakis (2006) developed a centerline model with fracturing connections. It allows for plastic hinge formation at the beam ends while the columns remain elastic. The specific model was used as a base-model for the current study, where the gravity system modelling was altered in such a way to permit the estimation of vertical floor accelerations at various locations of the floor. Figure 3-1 shows the plan layout of the building and a schematic structural elevation of the model. Table 3-1 shows the seismic weight at each floor, while Table 3-2 presents the MRF and gravity frame sections of the model. Gupta & Krawinkler (1999) provide sections for the gravity frame elements, and a single section for primary beams was selected across all floors. For the secondary beams, a W16×26 section was selected across all floors, spaced by 5ft.
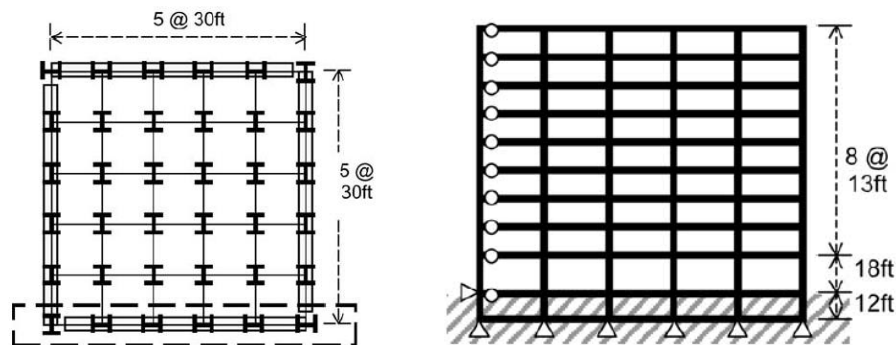
Figure 3-1: LA-9 building plan view (left) and MRF system (right) adopted from Foutch & Yun (2002)

Table 3-1: Elevation and seismic weights

Floor level	elevation (ft)	Seismic weight (kip)
1	18	2223
2	31	2185
3	44	2185
4	57	2185
5	70	2185
6	83	2185
7	96	2185
8	109	2185
9	122	2354

Table 3-2: Beam and column sections for the LA9 building

Story level	Seismic Frame			Gravity Frame	
	Column		Girder	Column	Beam
	Interior	Exterior	MRF		
-1	W14×605	W14×550	W40×183	W14×193	W21×44
1	W14×605	W14×550	W40×183	W14×193	W21×44
2	W14×550	W14×550	W40×183	W14×145	W21×44
3	W14×550	W14×550	W36×150	W14×145	W21×44
4	W14×550	W14×455	W36×150	W14×109	W21×44
5	W14×550	W14×455	W36×150	W14×109	W21×44
6	W14×455	W14×398	W33×118	W14×82	W21×44
7	W14×455	W14×398	W33×118	W14×82	W21×44
8	W14×398	W14×342	W27×94	W14×48	W21×44
9	W14×398	W14×342	W21×62	W14×48	W21×44

The effect of the concrete deck on the stiffness of the primary and secondary beams was defined in terms of amplifying the beam's moment of inertia, I, such that it matches the inertia of the composite section *Icomp*. The inertia of the composite section for the primary and secondary beams, was estimated in SeismoStruct (2018). The material properties of the concrete and steel are presented in Table 3-3.

Table 3-3: Material Properties

E_C (ksi)	E_s (ksi)
3605	29000

The effective width of the slab, b_{eff}, was estimated based on AISC (2010) recommendations, where the effective width at each side of the beam is taken as the minimum between the half of the distance of subsequent beams, and *L/8*, namely:

$$b_{eff.i} = min\left(\frac{L}{8}, \frac{spacing}{2}\right)$$ (3.1)

Table 3-4: Composite section characteristics

Beam section	$h_{concrete}$ (in)	b_{eff} (in)
Primary	5.5	75
Secondary	5.5	60

After estimating the composite moment of inertia, *Icomp* from SeismoStruct, the moment of inertia of the primary beam section w21×44 is multiplied by 3.3 to account for the effect of the slab, while the secondary beam's moment of inertia is multiplied by 3.6. The primary beam, which is added to the OpenSees model, is illustrated in Figure 3-2. The left panel of this figure displays the plan view of the primary and secondary beams, with the latter placed in a "binary" fashion, not to overstress the middle primary beam. On the right panel of this figure, the vertical mass that goes to the primary beam is illustrated with the purple solid area. The bottom purple solid area, is the mass that goes to the MRF system, while the remaining mass goes to the gravity system. The gravity system is comprised by 8 gravity columns and 4 MRF columns of the perimeter frames on the perpendicular direction.

The primary beam to column connection is assumed to be pinned. The primary beam is discretized in 6 segments, and nodal masses are assigned based on tributary lengths, as seen in Figure 3-3, with the red dashed line indicating the mass distribution to each node. The vertical period of this primary beam, with the modified moment of inertia *I* due to composite action, the specific line mass, and the boundary conditions with the column being pinned, is T=0.165s. Figure 3-4 shows the plan view of the secondary beams. The blue lines indicate the secondary beams which are spaced by 5ft, while the green lines

indicate the primary beams, and the red dashed lines indicate the mass distribution to each secondary beam. The secondary beam to primary beam connection is assumed to be pinned. The vertical period of this secondary beam, with the modified moment of inertia, due to the composite action, the specific line mass, and the specific boundary conditions with the primary beam, is T=0.151s. More details regarding can be found in Appendix B.

In a 3D model, the mass is attached directly to the secondary beams-slab, and to the primary beams indirectly via springs, as shown in Figure 3-5. The total mass that goes to the primary beam has to pass through the secondary beams first. The mass, *m*, that goes from one secondary beam to the primary beam is half of the total mass of the secondary beam. The stiffness of the red springs (secondary beam spring) in Figure 3-5 is defined such that, for half of the mass of the secondary beam, the period of the spring is the period of the secondary beam, namely T=0.151s. The period of the secondary beam can be estimated either through running an eigenvalue analysis of a beam with distributed vertical mass along its length with the use of any finite element software, or through some empirical equations that estimate the vertical period of a beam, given the distributed mass, the boundary conditions of the beam, and the moment of inertia. Now, the 1st vertical period of the floor system depicted in Figure 3-5 corresponds to the primary and secondary beams acting in series, since the vertical mass is attached to two flexible springs, rather than one. The period of this system is estimated at T=0.22s.

 The primary beam is discretized to 6 *elasticBeamColumn* elements in OpenSees. All the nodes of the gravity system, along with the MRF system, are constrained horizontally to the leftmost node of the MRF system through the *equalDOF* command. The primary beam is supported by 2 gravity columns. The connection of the primary beam to the column is pinned. This is achieved through the use of a *zeroLength* spring with very low rotational stiffness and high shear stiffness. The axial degree of freedom (DOF) is carried out by the horizontal diaphragm at each floor level. The secondary beam springs (red springs) in Figure 3-5 are modelled as *zeroLength* springs, with high shear and flexural stiffness, with flexibility only in the axial direction. At each gravity column, an extra mass, *M* is assigned, which is the mass coming from the other 3 slabs surrounding the gravity column. This mass is not directly attached to the column, instead it is attached to it via an axial spring, which represents the 1st period of the slabs system (T=0.22s). This is justified because the mass is directly attached to the secondary beams, and indirectly to the primary beam and column. It is like having a system of a secondary beam, primary beam and column in series. Thus, the spring attached to the column (blue spring) in Figure 3-6, has an axial stiffness such that, for the corresponding mass (¾ of the mass that goes to each gravity column, because the other ¼ goes through the primary beam that is already included in the model), it will have a period of T=0.22s (primary and secondary beam in series). This is achieved with *zeroLength* springs with high shear-rotational stiffness and flexibility only in the axial direction. The model configuration is illustrated in Figure 3-6. The floor system, along with

the remaining gravity columns, which are represented by a single leaning column, are connected to the MRF system via a horizontal diaphragm (Figure 3-7).

The gravity columns are continuous along the height of the structure, contributing to the horizontal stiffness of the structure. The horizontal DOF of the basement is fixed at the leftmost node of the MRF, with the horizontal diaphragm that is applied, fixing the entire basement horizontally. The base nodes at the ground are pinned. Vamvatsikos & Fragiadakis (2006) provide the details of the structural modelling of the MRF system. Eigenvalue analysis was carried out in OpenSees, while the following visualizations plots and the mass participation factors were derived through the use of the matlab software courtesy of Prof. Dimitrios Vamvatsikos.

Table 3-5: Vertical mode participation

Period	T(s)	$Meff_y$
4	0.324559	0.767411
7	0.241869	0.119488
9	0.230778	0.043788
11	0.227336	0.020169
15	0.225477	0.01375
46	0.15304	0.001245

The gravity beams are vibrating as simply supported beams. Their fundamental element-level mode shape is a half-sine represented by $\sin(2\pi x/L)$, where x in [0, L]. Within a single whole-building eigenmode, these individual beams can vibrate both in and out of phase in different combinations. This fact, creates a lot of similar modes of vibration, with very close periods, and phase difference between floors. The 4th eigenvector (Figure 3-8) represents the 1st vertical mode, with a period of T=0.32s which is the mode of the slab system and the gravity column acting in series. The column axial flexibility, especially at the top floors, is what makes the 1st mode more flexible than the period of the slab itself, which is at T=0.22s. The 7th eigenvector (Figure 3-9) has a period of T=0.24s, since it involves less contribution of the column axial deformation. The 34th mode (Figure 3-10) is the secondary beam mode with some flexibility of the primary beam, vibrating on its 2nd mode of vibration. The 42nd mode (Figure 3-11) is the secondary beam mode with some flexibility of the primary beam, vibrating on its 3rd mode shape.

At this point, 2% damping ratio is assigned to the 1st and 5th mode (Figure 3-12). The specific damping assumption was made for two reasons. First of all, the structure is a steel moment-resisting frame, and secondly, since it is an open-space building without partition, the vertical modes of vibration do not have the extra source of damping coming from the partitions. The 1st vertical mode corresponds to the mode of primary-secondary beam and column in series. The 2nd vertical mode corresponds to the mode of primary and secondary beam in series. The 3rd vertical mode is the mode of the secondary beams alone (in series with the higher modes of the primary beam). In that way, the vertical modes have reasonable damping values (less than 5%). The validation of the OpenSees model via comparison with the results of modal analysis done in SAP2000 is presented in the Appendix B.
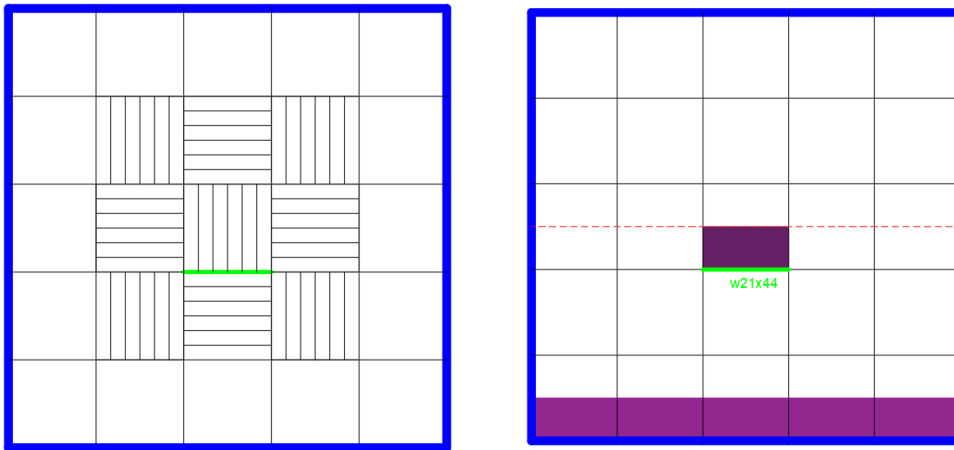
Figure 3-2: Plan view of primary-secondary beams (left), vertical mass distribution to the primary beam (right)
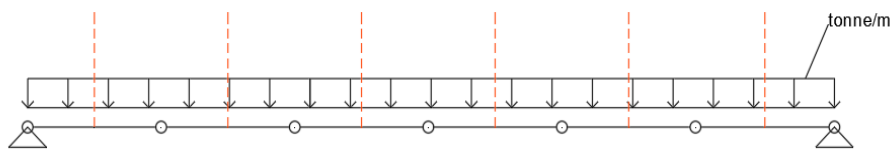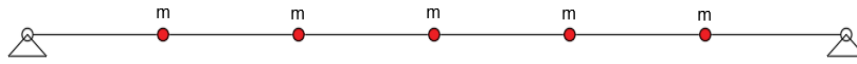
Figure 3-3: Vertical mass distribution to primary beam, with m being the nodal vertical mass

w16x26

w21x44
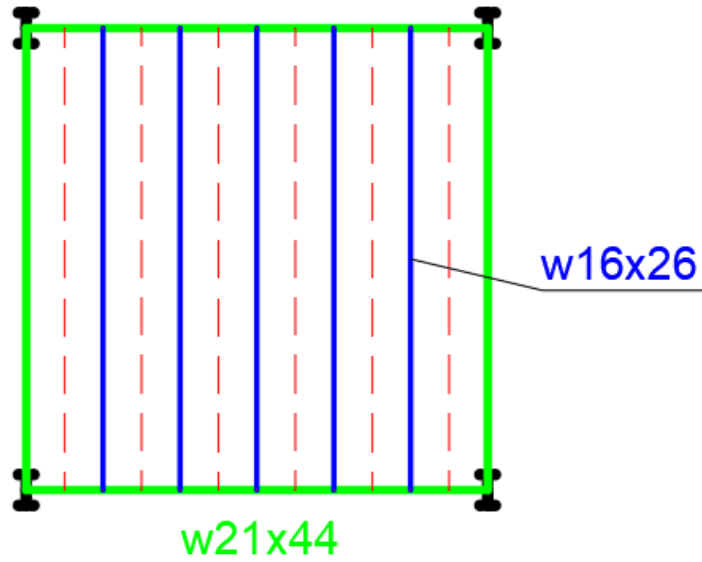
Figure 3-4: Plan view of Secondary beams
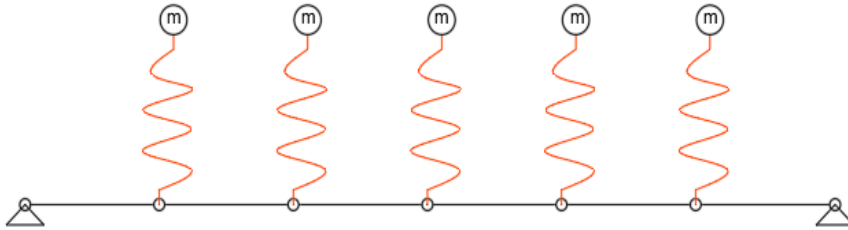
Figure 3-5: Vertical mass indirectly attached to the primary beam via the secondary beam springs
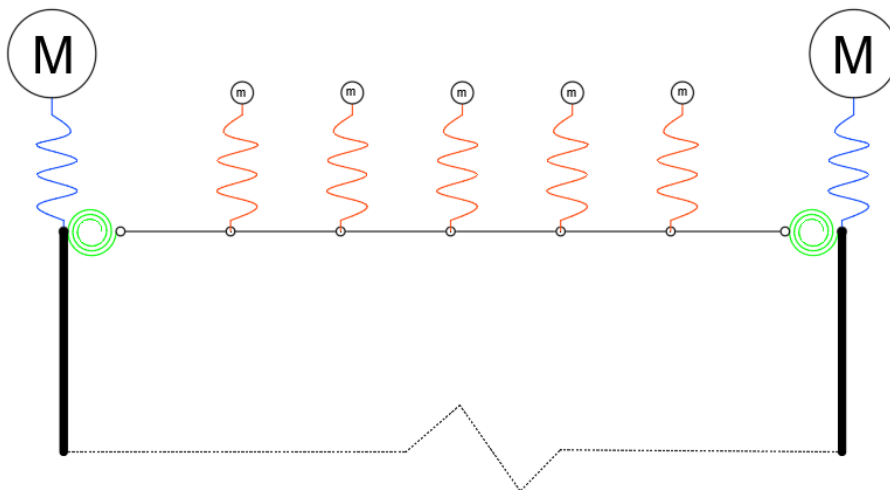
Figure 3-6: Floor system modelling configuration
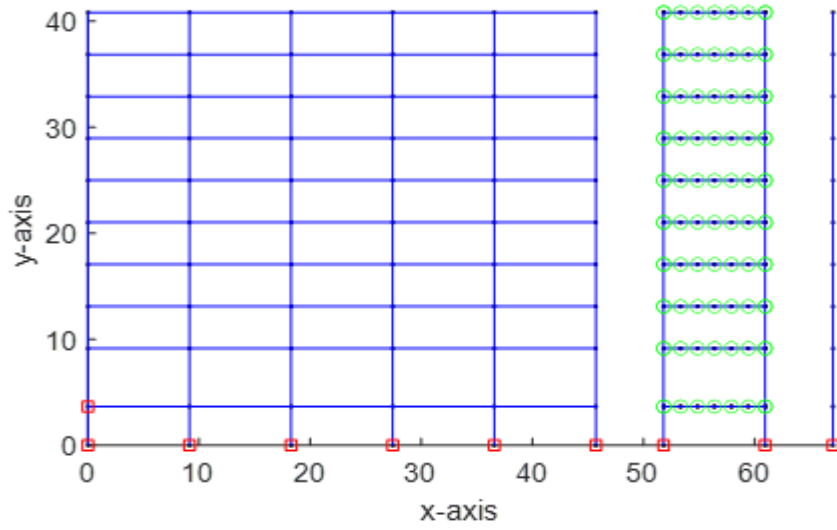
Figure 3-7: OpenSees model
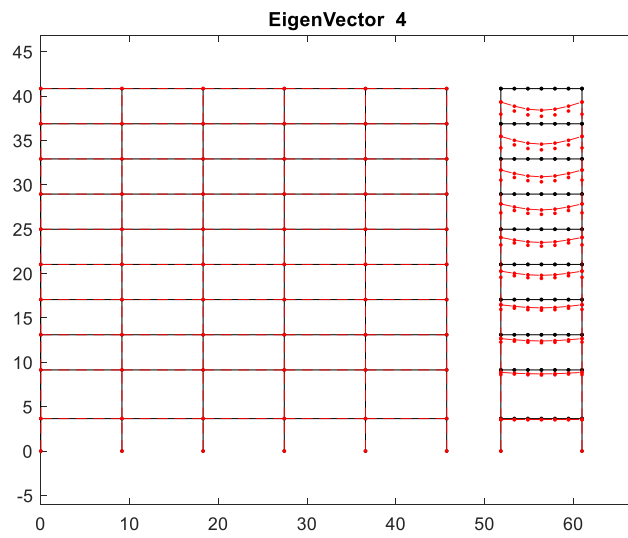
Figure 3-8: 4ᵗʰ Eigenvector-T=0.32s Slab acting in series with the gravity column axial deformation
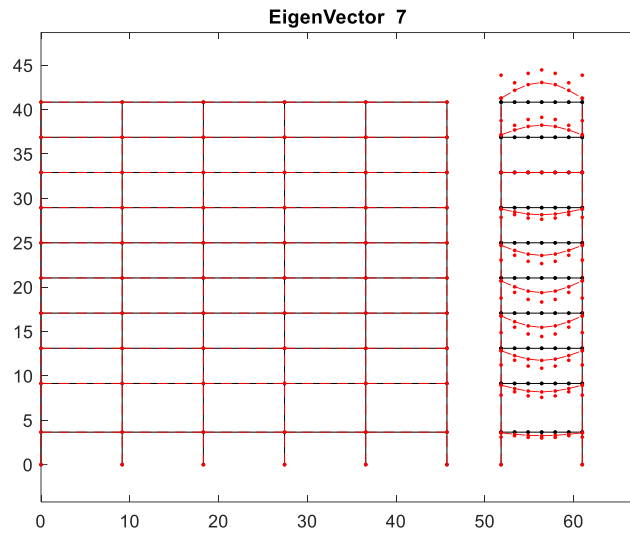
EigenVector 7

Figure 3-9: 7th Eigenvector-T=0.24s

EigenVector 34
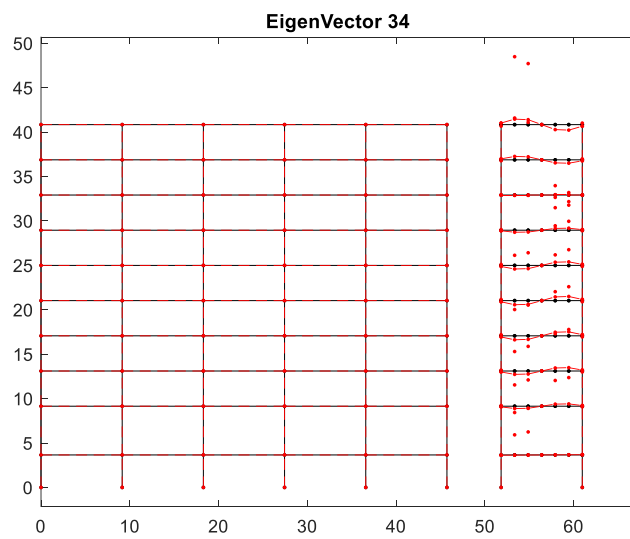
Figure 3-10: 34th mode-T=0.158s -secondary beam mode
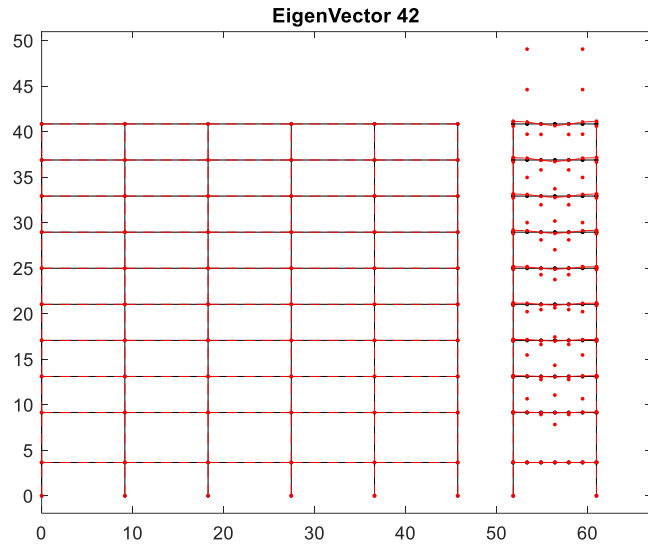
Figure 3-11: 42ⁿᵈ mode -T=0.153s- secondary beam mode
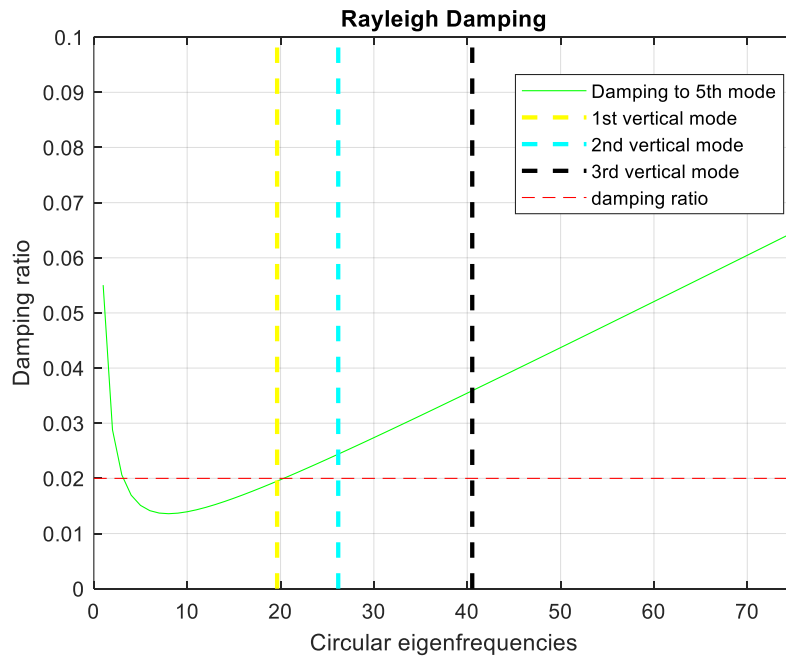
Figure 3-12: Rayleigh Damping

3.3 GROUND MOTION DATABASE AND NONLINEAR DYNAMIC ANALYSIS

The ground motion database used for this study is described in the section 2.3. The model is exposed to the bidirectional set of ground motions. The horizontal floor accelerations at each floor, along with the vertical floor accelerations at various locations of the floor are computed. In Figure 3-13 the vertical floor acceleration time history at the gravity column (top figure), and the open bay (bottom figure) are presented. The vertical component of ground motion is rich in the high frequency content, resonating with the important vertical modes of the structures which have low periods of vibration, resulting in high amplification factors for the vertical accelerations.
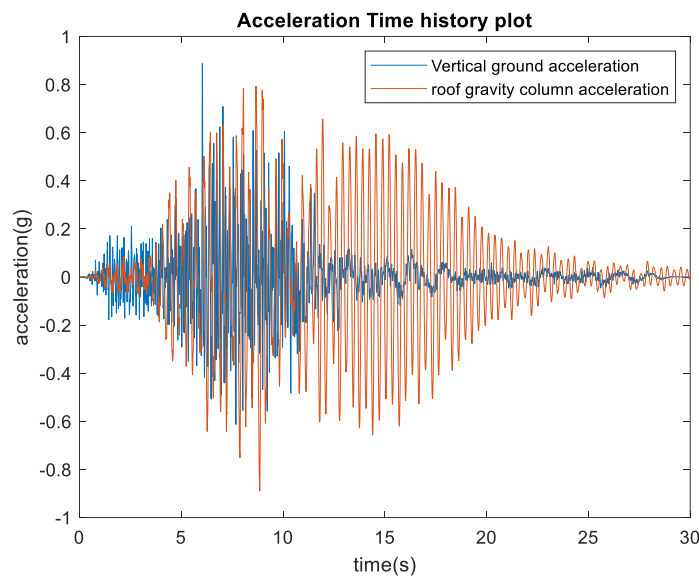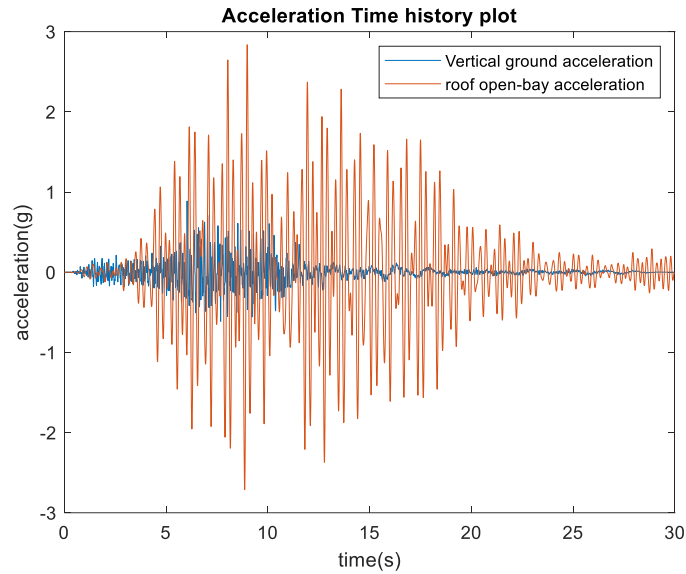
Figure 3-13: Vertical floor acceleration time history plots along with the vertical ground acceleration -IM6/Chi-Chi 1999, Sequence number=3176 from NGA-West

3.4 PROBABILISTIC ANALYSIS OF THE FLOOR ACCELERATION DEMAND

The results of the Multiple Stripe Analysis (MSA) are presented here. The peak floor acceleration demand for both horizontal and vertical direction are assessed in a probabilistic manner. Figure 3-14 shows the profile (along height of the building) in terms of the median amplification of the vertical acceleration at various IM levels. It is seen that it is quite similar for all IM levels, since the vertical response is elastic and it is not affected by the ductility demand of the structure.

Figure 3-15 shows the amplification by height of the vertical acceleration at the gravity column location for IM 7, with the accelerations being normalized with respect to the top of the basement. It is important to note, that the vertical mass of pertinence to the basement beams, and the basement column, does not have impact on the global response of the structure, since the basement columns are axially rigid. Although the vertical mass was introduced to the basement model, the normalization plots are taken with respect to the top of the basement for simplicity. The same applies for Figure 3-16 where the amplification by height of the vertical acceleration for IM7 at the open-bay location is shown. Because there are no ceilings at the basement, the normalization is assumed to take

place with respect to the top of the basement for simplicity (assuming that the vertical ground acceleration is the same as the top of the basement).

The amplification of accelerations at the gravity column is more pronounced at the upper floors, where the columns are less axially rigid. If the gravity column mass had been directly attached to the columns, and not via a flexible spring representing the flexibility of the slab, then the amplification at the top floors would have been much higher, and this would have affected the open-bay estimates as well. In that way the column axial deformation would have been forced to take all the vertical motion. Since the gravity column mass is supported by two springs in series (primary-secondary beam and the column axial deformation), then the relative flexibility of these springs is critical for the response.

If the gravity column was perfectly rigid, or the slab system was very flexible compared to the gravity column axial deformation, then the column would not have had much influence on the results of the open-bay. In the specific case of the LA9 building, where the top floors have axially flexible columns at the top floors, their importance for the response is relatively high. By looking at Figure 3-16, it can be observed that the open-bay acceleration at the top floors is increased compared to the lower floors, and this has to do with the column axial flexibility. Since the gravity columns of the top floors are more flexible, the acceleration is amplified at the upper part of the structure.

The vertical floor accelerations (Figure 3-18) and the amplification factors at the primary beam level (Figure 3-19) are lower than those in the secondary beam (Figure 3-20), since the secondary beam further amplifies the motion of the floor. The PFA_v amplification factors are similar across all IM levels since the vertical response is elastic and it is not affected by the ductility demand of the structure.

The horizontal floor acceleration amplification at roof is presented in Figure 3-21. The structure is horizontally flexible with a fundamental mode of T=2.01s, which indicates that it does not experience high floor accelerations even for elastic response. As the intensity of the ground motion increases, horizontal acceleration deamplification is observed, due to the structure's yielding and this prevents the horizontal floor acceleration to increase much, compared to the horizontal ground acceleration. Figure 3-22 shows the amplification of the vertical acceleration at the roof/open bay, compared to the horizontal acceleration amplification at the roof. We can see that the median translates to the right as the intensity level increases, since at those high IM levels, the horizontal acceleration tends to be deamplified.
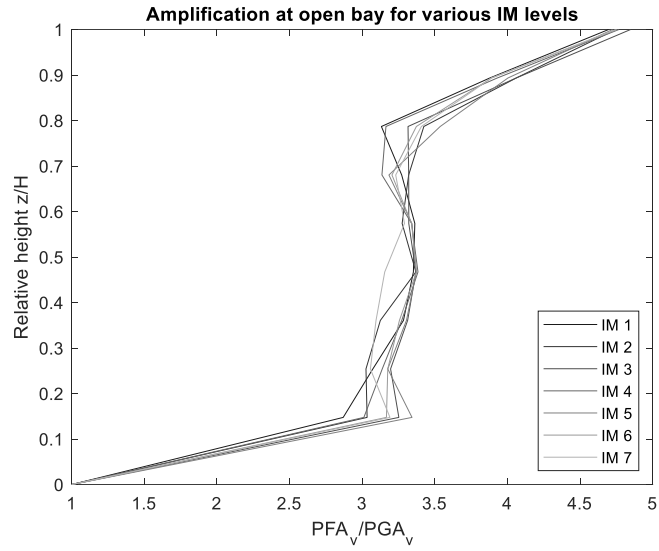
Figure 3-14: Vertical floor acceleration amplification by height at open-bay for various IM levels
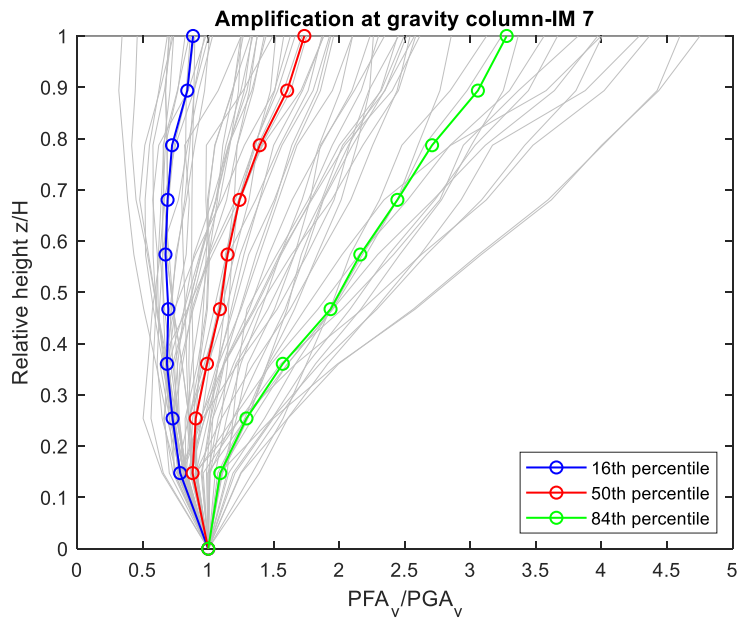
Figure 3-15: Vertical floor acceleration amplification by height at gravity column
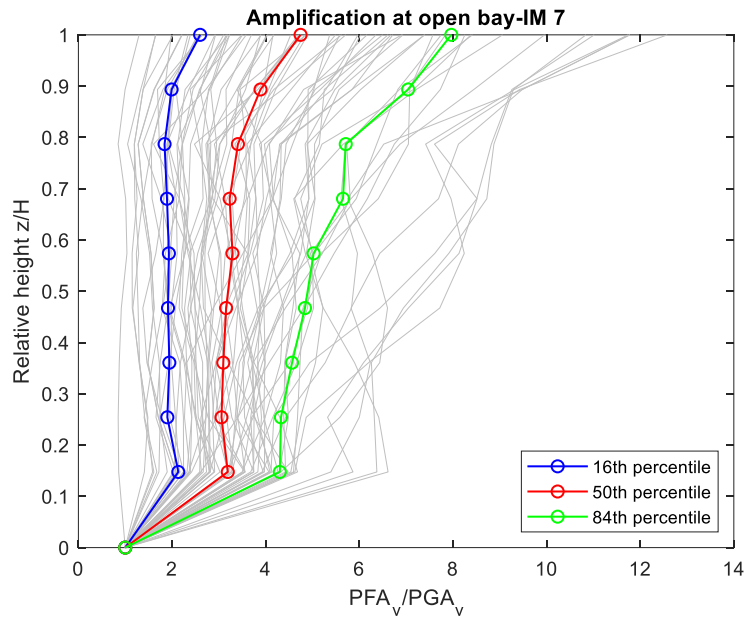
Figure 3-16: Amplification of the vertical floor acceleration by height at open-bay
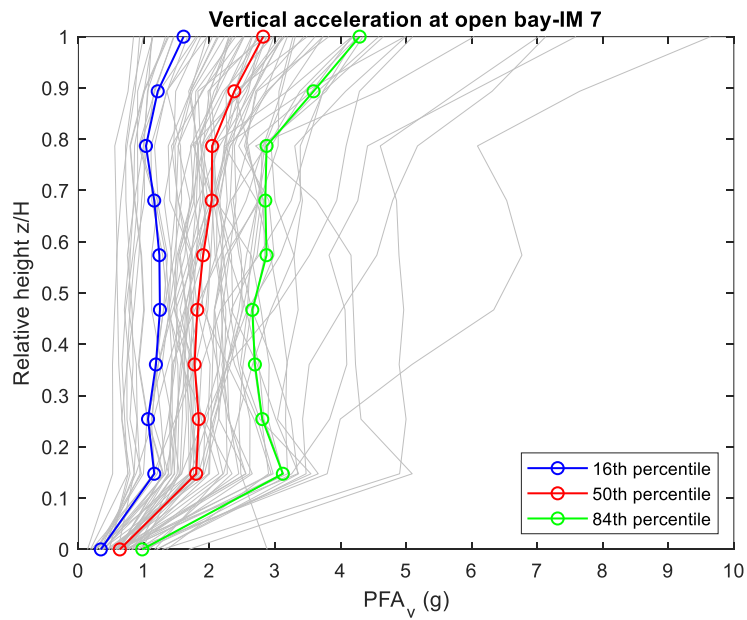
Figure 3-17: Vertical floor acceleration by height at open-bay
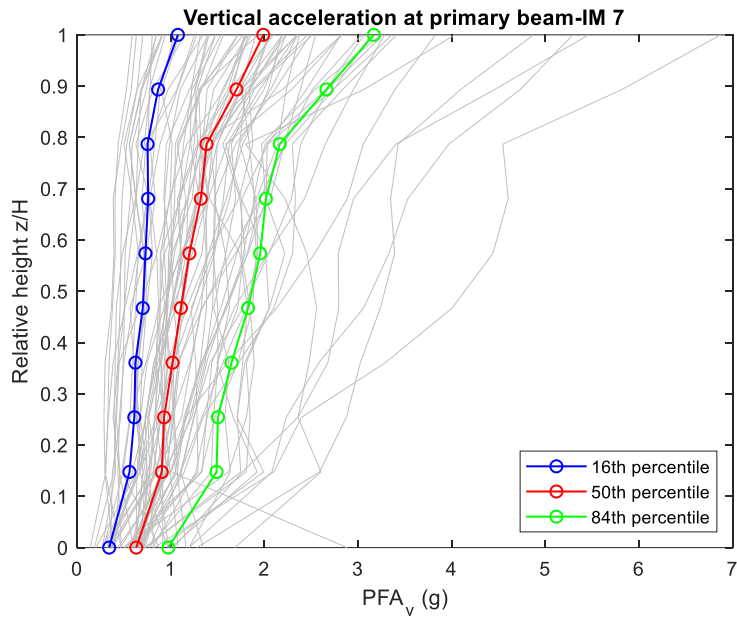
Figure 3-18: Vertical floor acceleration by height at primary beam
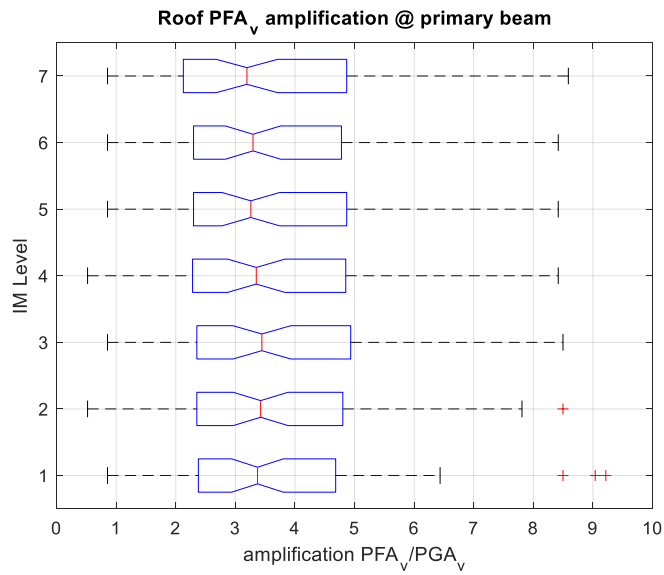
Figure 3-19: Amplification of the roof vertical acceleration at primary beam for various IM levels
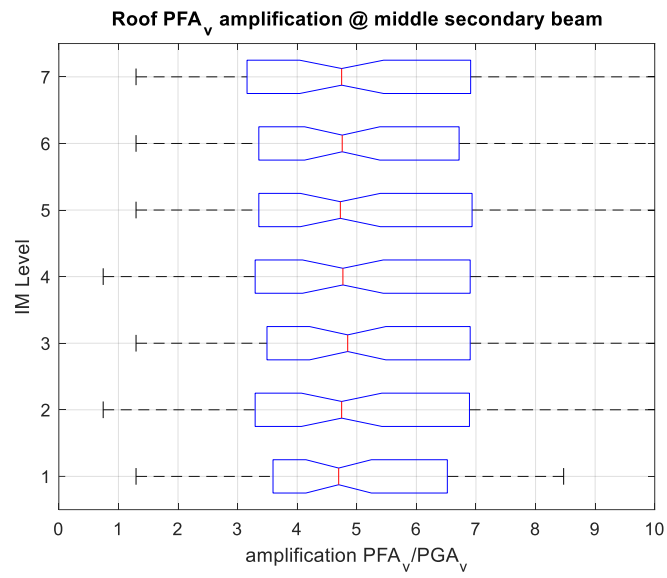
Figure 3-20: Amplification of the roof vertical acceleration at secondary beam for various IM levels
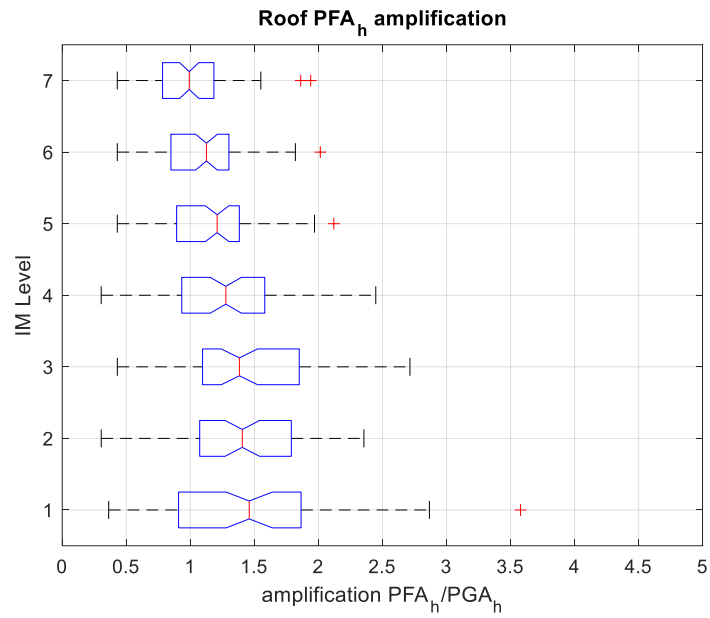
Figure 3-21: Amplification of the roof horizontal acceleration for various IM levels
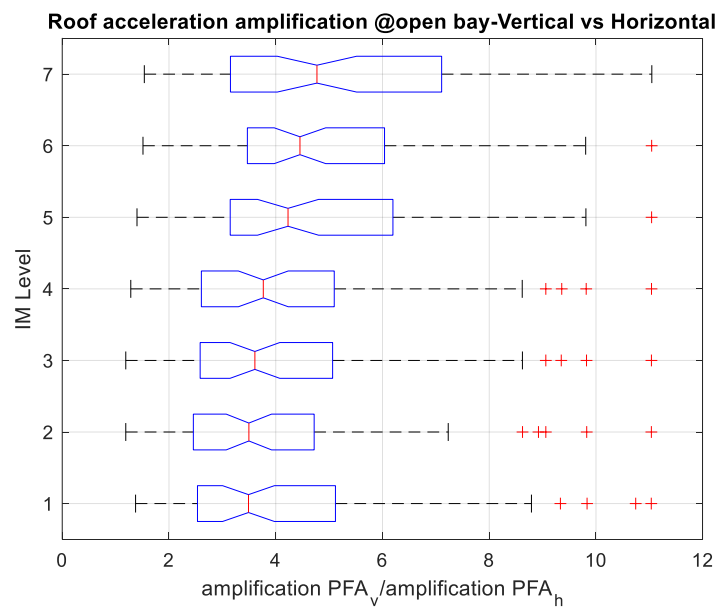
Figure 3-22: Comparison between Roof vertical and horizontal PFA amplification factors at open bay

3.5 LOSS ASSESSMENT OF THE CEILINGS

This section is dedicated to the development of a framework for loss estimation due to repair/replacement damage of, ceilings which are sensitive to both horizontal and vertical floor acceleration.

3.5.1 Framework

The fragility curves for the horizontal floor accelerations were taken from Performance Assessment Calculation Tool (PACT) for horizontally and vertically braced ceilings with area, A>2500 square ft, seismic category (C, D, E, F) and importance factor Ip=1.5. This is an assumption for ceilings of open-space office building with no partitions. Damage state 1 is characterized by 5% ceiling grid and tile damage, DS2 by 30% ceiling grid and tile damage, while DS3 by 50 % grid and tile damage. Table 3-6 shows the horizontal floor acceleration fragility parameters derived from PACT.

Table 3-6: PFA$_h$ fragility parameters

Damage State	PFA$_h$ (g)	β
DS1	1.31	0.3
DS2	2.03	0.3
DS3	2.29	0.3

Ryan et al (2016)   derive some performance criteria for the vertical floor acceleration fragility parameters from a large-scale experiment, in which a base isolated structure was exposed to both horizontal and vertical ground motions. The purpose was to define fragility criteria for ceilings against the vertical floor acceleration, since the base isolation would constrain the horizontal floor acceleration at low levels. The ceiling system used in this experiment had an area of A=900 square ft, and was seismically designed for Seismic categories C, D, E, F. Three damage states are proposed for the vertical floor accelerations (Ryan et al., 2016). Soroushian et al (2016), describe the failure damage modes, where it is mentioned that the most vulnerable ceilings against the vertical component appear to be the vertically braced ceiling. Moreover, a very important failure mode is the pounding of the fire-sprinkler head with the ceiling panels, and this failure mode is observed in both vertically braced and unbraced ceilings. This is the reason why the acceleration limits proposed in those studies apply to both braced and unbraced ceilings. There were also some other failure modes observed, regarding the perimeter seismic clip, pounding, etc.

Ryan et al. (2016) define the onset of damage states DS1, DS2, DS3 at 2g, 3g and 5g vertical acceleration respectively. In the current study, we assume these values as the medians of the lognormal fragility distributions of the ceilings in terms of the vertical floor acceleration. Furthermore, a logstandard deviation β, is assumed to be 0.3. The assumed vertical floor acceleration fragility parameters are shown in Table 3-7.

For the vertical acceleration fragilities, according to Ryan et al (2016), DS1 means ceiling panels up to 5% equivalent area fall, along with slight damage to panels from pounding between the sprinkler head and the ceiling panel. Damage State 2, means panels between 5 and 20% equivalent area fall, more significant damage to panels at sprinkler heads because of pounding interaction, some cross-tee fail, and ceiling hanger wire breakage. Damage state 3 means ceiling panels exceeding 20% equivalent area fall, grid components buckling, and connection failures very significant damage to panels from the pounding with sprinkler heads, along with significant damage to piping system. Figure 3-23 show the horizontal floor acceleration fragility for suspended ceilings, and Figure 3-24 show the vertical floor acceleration fragility for suspended ceilings.

Table 3-7: PFA$_v$ fragility parameters

Damage State	PFA$_v$ (g)	β
DS1	2	0.3
DS2	3	0.3
DS3	5	0.3
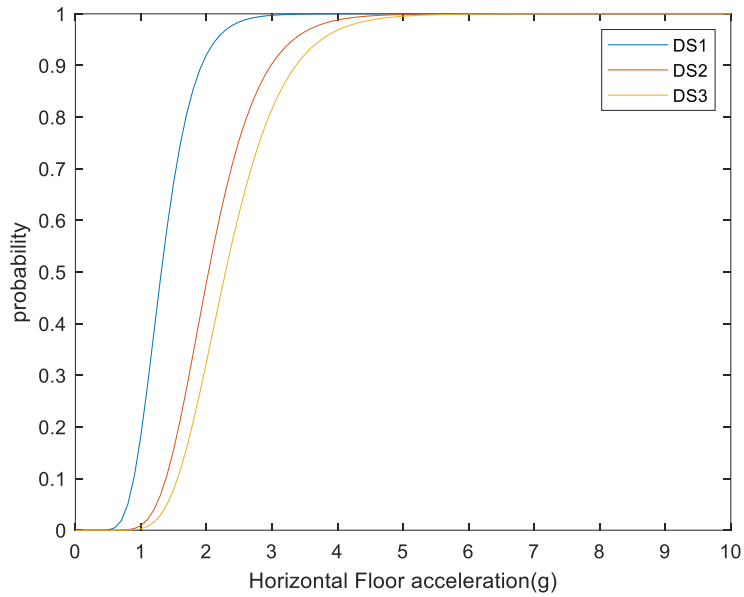
Figure 3-23: Horizontal floor acceleration fragility for suspended ceilings
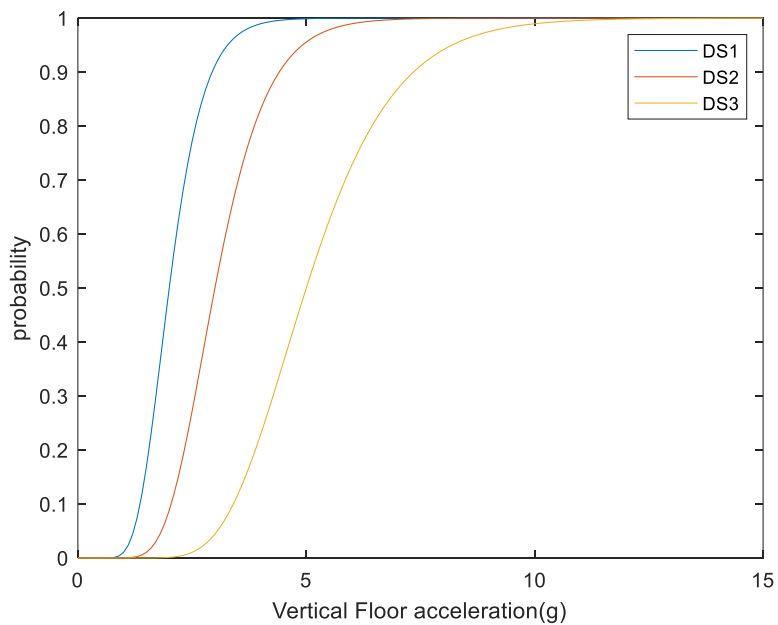
Figure 3-24: Vertical floor acceleration fragility for suspended ceilings

From the NLTHA, the predictors that are going to be used for the loss estimation of the ceilings are, the peak horizontal acceleration at each floor, and the peak vertical acceleration at each secondary beam of each floor. Each secondary beam has a tributary area denoted by the red dashed lines (Figure 3-25). Each of these ceiling areas will vibrate with the vertical acceleration of the corresponding secondary beam. The assumption made here is that the areas beyond the red dashed lines will vibrate with the vertical acceleration of the exterior secondary beams. Another assumption is that the exterior slabs (those that connect the gravity frame with the MRF system), will have similar acceleration to the gravity system slabs. Each of the 5 masses depicted in Figure 3-26, will have a specific vertical floor acceleration, and the same horizontal acceleration. At first, in the post-processing code, and for each IM level, ground motion, floor, and mass (secondary beam position), the probabilities that the ceilings at a given location of the building at the end of the shaking will be in DS_0, DS_1, DS_2, or DS_3 due to vertical acceleration are derived by means of the vertical acceleration fragilities derived in the previous pages. Moreover, for each IM level, ground motion and floor (since all 5 masses at each floor will have the same horizontal acceleration due to the horizontal diaphragm), the probabilities of the ceilings of being in DS_0, DS_1, DS_2, or DS_3 due to the horizontal acceleration are derived by means of the horizontal acceleration fragilities derived in the previous section. Since, no relevant data is available, interaction between horizontal and vertical accelerations is not accounted for.

For each IM level and ground motion record, 100 horizontal and vertical capacity realizations are performed. A range of numbers is assigned to each damage state, with DS_1 assigned a range from 1 to $(100 \times P(DS_1))$, DS_2 from $(100 \times P(DS_1)+1)$ to $(P(DS_1)+ P(DS_2)) \times 100$ and so on. A number is generated between 1-100 and the range in which it falls determines the damage state for the specific realization. Thus, for each realization the ceiling components at different locations of the floor (since we have 5 open-bay estimates per floor) will be assigned a horizontal and vertical damage state DS_h, and DS_v respectively. The horizontal-vertical damage state DS_{hv} for this particular realization is then defined as the worse between DS_h and DS_v.

The ceilings of each floor, will have a horizontal and a vertical capacity. We will consider four different options for modelling correlation among them. The first option is to assume perfect correlation between the horizontal capacities of different floors, perfect correlation between the vertical capacities of different floors, and perfect correlation between the horizontal and vertical capacity of each floor (Case 1). The second way is to assume perfect correlation between the horizontal capacities of different floors, perfect correlation between the vertical capacities of different floors, and zero correlation between the horizontal and vertical capacity of each floor (Case 2). The third option is to assume zero correlation between the horizontal capacities of different floors, zero correlation between the vertical capacities of different floors, and perfect correlation between the horizontal and vertical capacity of each floor (Case 3). The fourth choice is to assume zero correlation

between the horizontal capacities of different floors, zero correlation between the vertical capacities of different floors, and zero-correlation between the horizontal and vertical capacity of each floor (Case 4). The capacity correlation assumptions for all Cases, are summarized in Table 3-8. The capacities of the ceilings at different locations and at different floors comprise a random field. Since there is a random field, capacity correlations should be taken into account. The number generated from 1-100 corresponds to the capacity of the ceiling component. In order to control correlations between ceiling components, instead of randomly generating numbers between 1-100, stratified sampling is performed.

As stated earlier, the first way is to assume perfect capacity correlation between different floors and also perfect correlation between horizontal and vertical capacities at each floor. At each realization, a number between 1-100 is generated for the horizontal capacities of each floor (Table 3-9) and for the vertical capacities of each floor (Table 3-10). Since there is perfect correlation between the horizontal capacities of different floors, the numbers generated for each floor are the same (Table 3-9). Since there is perfect correlation between the vertical capacities of different floors, the numbers generated for each floor are the same (Table 3-10). Since there is perfect correlation between horizontal and vertical capacities at each floor, the numbers generated for each floor should be the same for both the horizontal and vertical capacities (Table 3-9, Table 3-10).

The second option is to assume perfect capacity correlation between different floors and zero correlation between horizontal and vertical capacities at each floor. At each realization, a number between 1-100 is generated for the horizontal capacities of each floor (Table 3-11) and for the vertical capacities of each floor (Table 3-12). Since there is perfect correlation between the horizontal capacities of different floors, the numbers generated for each floor are the same (Table 3-11). Since there is perfect correlation between the vertical capacities of different floors, the numbers generated for each floor are the same (Table 3-12). Since there is zero correlation between horizontal and vertical capacities at each floor, the numbers generated for each floor should not be the same for horizontal and vertical capacities (Table 3-11, Table 3-12). The zero-correlation between H-V capacities is achieved by random permutation of numbers.

The third option is to assume zero correlation between different floors and perfect correlation between horizontal and vertical capacities at each floor. At each realization, a number between 1-100 is generated for the horizontal capacities of each floor (Table 3-13) and for the vertical capacities of each floor (Table 3-14). Since there is zero correlation between the horizontal capacities of different floors, the numbers generated for each floor are not the same (Table 3-13). Since there is zero correlation between the vertical capacities of different floors, the numbers generated for each floor are not the same (Table 3-14). Since there is perfect correlation between horizontal and vertical capacities at each floor,

the numbers generated for each floor should be the same for both the horizontal and vertical capacities (Table 3-13, Table 3-14).

The fourth option is to assume zero correlation between different floors and zero correlation between horizontal and vertical capacities at each floor. At each realization, a number between 1-100 is generated for the horizontal capacities of each floor (Table 3-15) and for the vertical capacities of each floor (Table 3-16). Since there is zero correlation between the horizontal capacities of different floors, the numbers generated for each floor are not the same (Table 3-15). Since there is zero correlation between the vertical capacities of different floors, the numbers generated for each floor are not the same (Table 3-16). Since there is zero correlation between horizontal and vertical capacities at all floors, the numbers generated for each floor should not be the same (Table 3-15, Table 3-16).

Table 3-8: Ceiling capacity correlation assumptions

Case n.	Ceiling capacity correlation assumption
Case 1	Horizontal capacities between different floors are perfectly correlated. Vertical capacities between different floors are perfectly correlated. Horizontal and Vertical capacities at each floor are perfectly correlated.
Case 2	Horizontal capacities between different floors are perfectly-correlated. Vertical capacities between different floors are perfectly correlated. Horizontal and Vertical capacities at each floor are zero correlated.
Case 3	Horizontal capacities between different floors are zero-correlated. Vertical capacities between different floors are zero-correlated. Horizontal and vertical capacities at each floor are perfectly correlated.
Case 4	Horizontal capacities between different floors are zero-correlated. Vertical capacities between different floors are zero-correlated. Horizontal and vertical capacities at each floor are zero-correlated.

Table 3-9: Random numbers generated for the ceiling capacities for the horizontal component-CASE 1

Floor#	Realization #1	Realization #2	Realization #3	Realization #4	Realization #5
1	1	2	3	4	5
2	1	2	3	4	5
3	1	2	3	4	5
4	1	2	3	4	5
5	1	2	3	4	5
6	1	2	3	4	5
7	1	2	3	4	5

8	1	2	3	4	5
9	1	2	3	4	5

Table 3-10: Random numbers generated for the ceiling capacities for the vertical component-CASE 1

Floor#	Realization #1	Realization #2	Realization #3	Realization #4	Realization #5
1	1	2	3	4	5
2	1	2	3	4	5
3	1	2	3	4	5
4	1	2	3	4	5
5	1	2	3	4	5
6	1	2	3	4	5
7	1	2	3	4	5
8	1	2	3	4	5
9	1	2	3	4	5

Table 3-11: Random numbers generated for the ceiling capacities for the horizontal component-CASE 2

Floor#	Realization #1	Realization #2	Realization #3	Realization #4	Realization #5
1	1	2	3	4	5
2	1	2	3	4	5
3	1	2	3	4	5
4	1	2	3	4	5
5	1	2	3	4	5
6	1	2	3	4	5
7	1	2	3	4	5
8	1	2	3	4	5
9	1	2	3	4	5

Table 3-12: Random numbers generated for the ceiling capacities for the vertical component-CASE 2

Floor#	Realization #1	Realization #2	Realization #3	Realization #4	Realization #5
1	68	73	10	88	51
2	68	73	10	88	51
3	68	73	10	88	51
4	68	73	10	88	51
5	68	73	10	88	51
6	68	73	10	88	51
7	68	73	10	88	51
8	68	73	10	88	51
9	68	73	10	88	51

Table 3-13: Random numbers generated for the ceiling capacities for the horizontal component-CASE 3

Floor#	Realization #1	Realization #2	Realization #3	Realization #4	Realization #5
1	79	35	90	60	86
2	25	42	6	46	73
3	94	64	82	71	72
4	34	7	35	81	32
5	80	6	95	38	66
6	38	76	56	77	11
7	79	82	93	10	36
8	18	69	10	91	67
9	1	2	3	4	5

Table 3-14: Random numbers generated for the ceiling capacities for the vertical component-CASE 3

Floor#	Realization #1	Realization #2	Realization #3	Realization #4	Realization #5
1	79	35	90	60	86
2	25	42	6	46	73

3	94	64	82	71	72
4	34	7	35	81	32
5	80	6	95	38	66
6	38	76	56	77	11
7	79	82	93	10	36
8	18	69	10	91	67
9	1	2	3	4	5

Table 3-15: Random numbers generated for the ceiling capacities for the horizontal component-CASE 4

Floor#	Realization #1	Realization #2	Realization #3	Realization #4	Realization #5
1	11	2	22	24	36
2	84	57	69	6	19
3	47	83	16	95	80
4	42	6	52	5	53
5	71	52	19	37	41
6	53	10	55	49	80
7	11	94	91	89	98
8	92	23	100	30	12
9	1	2	3	4	5

Table 3-16: Random numbers generated for the ceiling capacities for the vertical component-CASE 4

Floor#	Realization #1	Realization #2	Realization #3	Realization #4	Realization #5
1	12	42	70	67	41
2	51	27	38	41	4
3	34	61	83	32	100
4	65	77	28	7	14
5	40	97	73	63	89
6	60	87	22	24	62
7	32	61	93	60	27
8	69	3	33	86	74
9	33	91	17	40	66

At this point, for each IM level, ground motion record, floor, and mass, there is a damage state assigned to each one of the ceilings caused by the vertical component, and a damage state assigned to it caused by the corresponding horizontal component. In order to take into account the presence of both the horizontal and vertical component, at each mass (secondary beam), a final damage state is assigned, DS_{hv}, which is taken as the worse of the two DS_h and DS_v. For example, for a specific realization, if the damage state due to the horizontal component of the ceilings at a given floor is DS_0 and, the damage state due to the vertical motion for a particular mass of this floor is DS_1, then the DS_{hv} will be taken as DS_1 for this particular mass.

The unitary repair cost for each damage state is taken from the PACT software for the specific type of ceilings, by assuming the maximum repair value from the cost function. The assumption made here is that the repair costs for both the horizontal and vertical damage states are the same, since there is little information that allows one to differentiate them (Table 3-17). The distributions of the repair cost per 2500 ft² are shown in Figure 3-27. Since the cost distribution is normal, with unbounded left tail, some negative cost values may occur, and these are censored to become zero. The total replacement cost of all the ceilings of the building is 9,456,750 $.

At each realization a random number is generated from the standard normal distribution, and then this number is used to estimate a cost for each damage state for this particular realization. In this way, by taking the same percentile for all damage states, if a realization is expensive (i.e., much larger than the median), it will be expensive for all damage states. Then, for each realization, floor and mass since there is a DS_h, DS_v and DS_{hv} assigned, a unitary cost is also assigned, $Cost_h$, $Cost_v$ and $Cost_{hv}$ respectively. The unitary cost, $Cost_h$ applies to the entire floor area, while the unitary costs $Cost_v$, $Cost_{hv}$ apply to the ceiling area of each vertical mass separately (Figure 3-25). By multiplying by the specific area, and summing up the repair costs of all the masses and floors for each realization, the total ceiling loss of the entire building is estimated, for the specific realization. For each realization, LossH (Loss due to horizontal acceleration only), LossV (Loss due to vertical acceleration only) and LossHV (Loss due to combined horizontal and vertical acceleration) of the entire building are estimated.

Figure 3-25: Slab system configuration
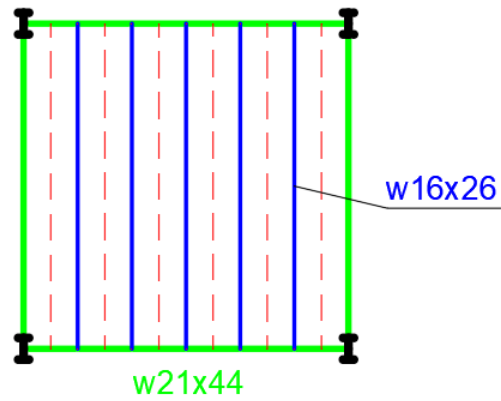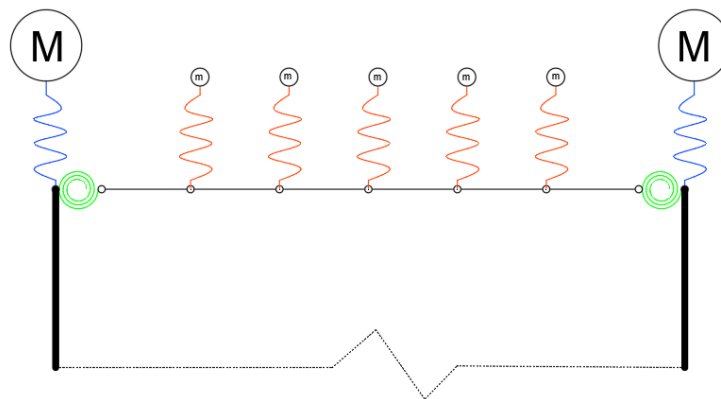

Figure 3-26: Floor system configuration

Table 3-17: Unitary Repair cost distribution

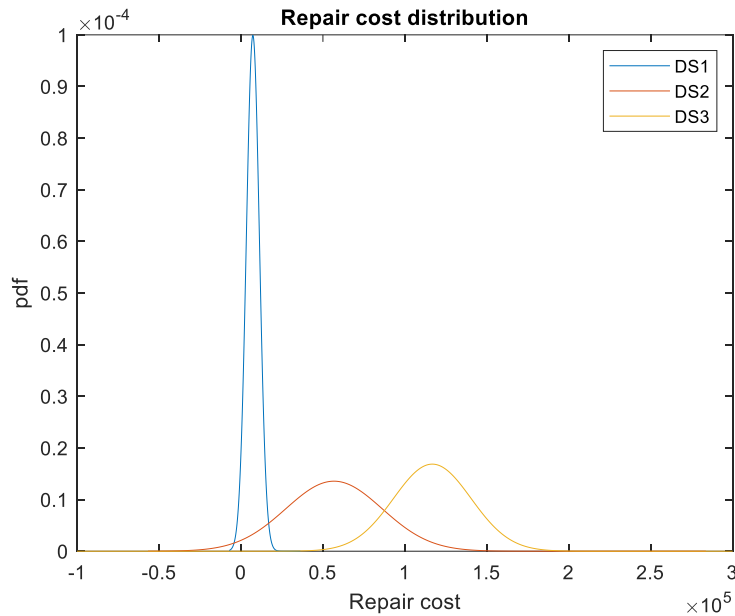|	μ($)	COV
DS1	7250	0.5508
DS2	56750	0.5183
DS3	116750	0.2026

Figure 3-27: Unitary repair cost distribution

3.5.2 Results Discussion

Since there are 7 IM levels, 70 ground motion per IM level, and 100 realizations of the losses caused by each ground motion, the data derived are enough to build fairly robust loss statistics. The building loss is modeled as a mixed random variable. For the histograms of the following pages, a bin close to zero-loss has been created. There are a lot of realizations with zero loss, which comes from the fact that for a particular realization, the ceilings might be undamaged since they are quite strong, or because the repair cost that has been sampled is zero. Hence, there might be cases where zero loss has a large concentrated mass. In that way this extra bin, will help to better visualize the histogram of the mixed random variable distribution. The results are discussed in 4 separate sections, depending on the capacity correlation assumption case. The histograms presented in the following pages are referred to the ceiling loss for IM 7, since this IM level is enough to present and interpret the results.

At first, Case 1 is discussed. As it is seen in Figure 3-28 , the zero-loss has a very large concentrated mass in the case of applying only the Horizontal component, with 0.53 frequency, while the zero-loss for the HV case is smaller, with a frequency of 0.22. This happens because the horizontal PFA's, are not as large as the PFAv's, for IM level 7, and

this results in the zero-loss having much less mass in the case of HV. Moreover, because the horizontal accelerations cannot go very high, due to the structure being flexible horizontally, and also due to the yielding of the structure, while the vertical component amplification factors are much higher at all IM levels, then, there is more mass on the right tail of the loss distribution in the HV case. By looking at Figure 3-29, it is seen that the LossHV and LossV distributions have very similar mass on the right tail, which indicates that the horizontal component will not affect much the extreme losses, while the inclusion of the horizontal component along with the vertical will give rise to higher losses on central values of the distribution. Also, the HV case has less zero-loss mass, than in the case of V only.

Secondly, Case 2 is discussed. Looking into Figure 3-30, the LossHV has less zero-loss mass compared to Case 1. Comparing Figure 3-31 and Figure 3-29, it seems that the right tail of the LossHV distribution is quite the same. This happens because at the right extreme, the LossHV and the LossV are quite the same. By putting zero correlation to H-V capacities, this tail will not change much. However, the zero-correlation case will give less mass to the left extreme as well, which is the concentrated zero-loss mass, and this effect will give higher probability mass to all the other values of the continuous distribution (mixed random variable). In the zero-correlation case the sampling will give more mass to the median values that's why the LossHV is higher than the LossV, compared to the perfect correlation case in Figure 3-29.

Case 3 is discussed herein. In Figure 3-32, it is seen that the zero-loss mass for the H case, is much less than in Cases 1, 2 where the LossH has more than 0.5 frequency concentrated on the zero-loss value. Comparing Figure 3-33 and Figure 3-31, it seems that the concentrated mass on zero-loss for the V case is much less in the case of zero-correlation between different floors. The LossH and LossV will have much less concentrated mass at the zero-loss in the case of zero-correlation between different floors.

Case 4 is the extreme case, it denotes zero-correlation among capacities at different floors, while there is zero correlation between H-V capacities at each floor as well. Comparing Case 3, and Case 4, there is slightly less mass concentrated on the zero-loss in Case 4 (Figure 3-34) than in Case 3, since there is zero H-V capacity correlation. Comparing Case 4 and Case 2, it seems that the appearance of H, on the LossHV distribution is increased (Figure 3-35) due to the higher decrease of the concentrated mass of the zero-loss for the H case, compared to the decrease of the concentrated mass of the zero-loss for the V case.

Seismically designed ceilings, are considered very strong components, which is reflected by the relatively low losses even for high IM levels. Figure 3-36 presents the median LossHV, LossH, LossV, for different IM levels, and different correlation assumptions. The median LossH, LossV are higher in the cases of zero-correlation between different floors. The loss

percentiles are affected by the assumptions made on the correlation capacities, namely either perfect or zero. The perfect correlation case, tends to sample in such a way that the extreme values of the final distribution will have more mass, and less mass will go to the central-median values. Plus, in the zero-correlation case, since the extremes will be sampled less, the concentrated mass on the zero-loss value will be less, and this effect, will give an extra mass to all the other values of the continuous distribution. Across all IM levels, the median LossH, LossV are higher for the zero-correlation case between different floors. Since, the median LossH, LossV are higher in the case of zero-correlation between different floors, the median LossHV is going to be higher in cases 3 and 4 (zero correlation between different floors), than in cases 1 and 2 (perfect correlation between different floors). The median LossHV, is higher for case 4, compared to case 3, since, in the latter, there is more concentrated mass on the zero-loss value. It is worth-mentioning that the median LossV for the case of zero-correlation between different floors is higher than the LossHV for cases 1 and 2 (perfect correlation between different floors), since in these cases the median is weaker.

The 84th percentile (Figure 3-37) is affected by two opposing effects: the first being, whether the correlation is perfect or zero, and second, the concentrated mass on zero-loss (which, again, it depends on the correlation assumption, as stated earlier). One should expect the H 84th percentile to be higher in the case of perfect-correlation, since the extremes are highly sampled. However, since the concentrated mass on the zero-loss is smaller in the case of the zero-correlation, this means that all the other values of the LossH distribution will gain more mass. This is the reason why, across all IM levels, the LossH for the case of zero-correlation among different floors is higher than in the case of perfect correlation. The same applies for the LossV across IM levels 1-6. However, in IM level 7, the LossV for the perfect correlation case, is the same as the zero-correlation case. This means that the effect of sampling the extreme values of the distribution counteracted the effect of the concentrated mass on zero-loss. This is an indicator that at this IM level, the extreme right tail became stronger than in the lower IM levels. Concerning the LossHV, from IM 1 to 6, the zero-correlation cases give higher values for the 84th percentile LossHV, with the Case 4 (zero-correlation among different floors, and zero-correlation between H-V capacities), having the higher values, since it has the less concentrated mass on zero-Loss. At IM level 7, the cases 1 and 2 become dominant, since the extreme right tail at this intensity level becomes stronger and overrides the effect of the concentrated mass on zero-loss. The LossHV at IM 7, of case 2 (zero-correlation between H-V capacities) is higher than that of case 1 (perfect correlation between H-V capacities), since case 2 has less concentrated mass on zero-loss compared to case 1.

Moreover, it is observed that the LossH increases with increasing intensity of the ground motion. This means that the horizontal PFA's increase with increasing IM. This is attributed to the fact that this model is strong and the nonlinearity is not so evident in the

high IM levels, which would cause the PFAh's, and thus the LossH, to saturate at higher IM levels. Plus, another reason might be that as the intensity level is increased, more and more records are going to damage the ceilings, leading to higher overall losses. As a general comment for the two trends (correlation & zero loss mass) affecting the extreme right loss, 84th percentile, it is worth mentioning that the left tail of each individual "floor" damage distribution is stronger than the right tail, because the ceilings are quite strong components, and even for high IM levels, the probability of no zero or Slight damage at a given floor is much higher than the probability of complete damage. Thus, the left tail of each individual damage distribution will be sampled more than the right tail when the total ceiling loss is estimated.

Moreover, the loss estimates, seem to be affected more by the correlation assumption between different floor capacities, than from the correlation between H, V capacities. This is due to the fact that in the case of the perfect correlation among different floors, since there are 9 different floors, more extreme values will be sampled from the individual damage distributions, while from the perfect correlation between HV, and zero among different floors, the LossH, LossV will not change, but only the LossHV.
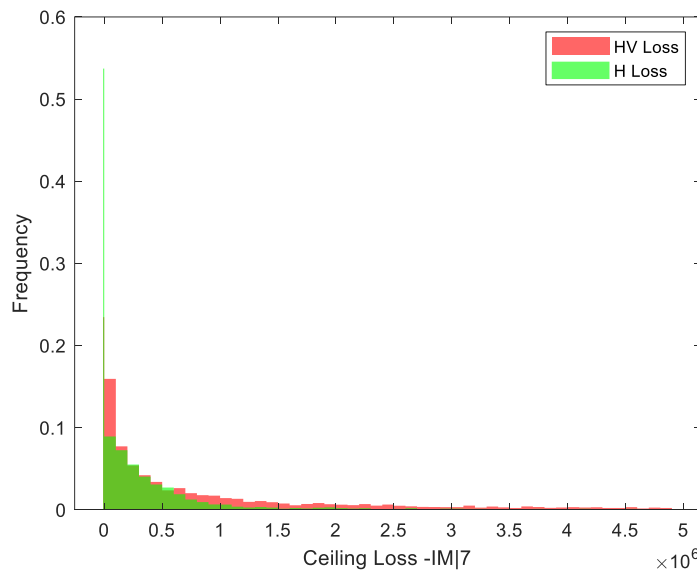

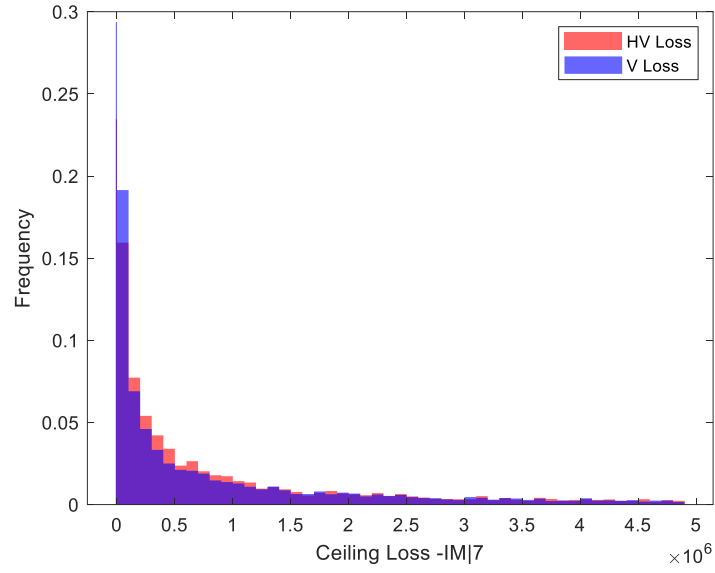**Figure 3-28: Histogram-Comparison of HV, H Loss-IM7-CASE 1**

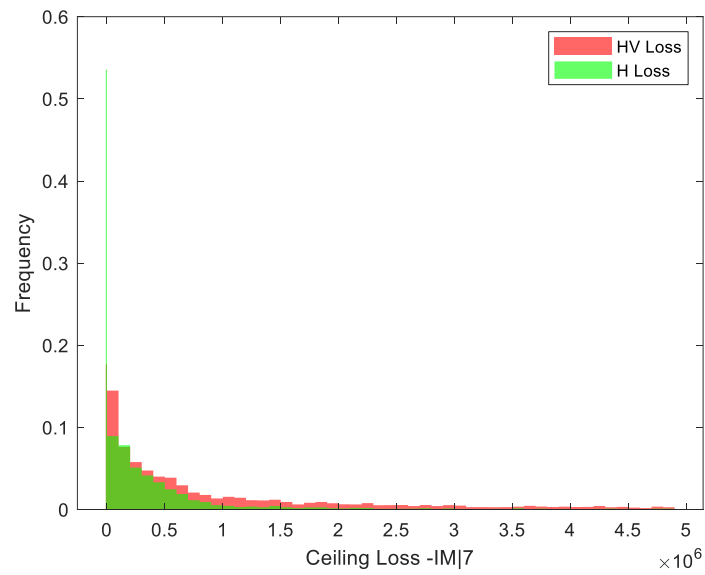**Figure 3-29: Histogram-Comparison of HV, V Loss-IM7 -CASE 1**

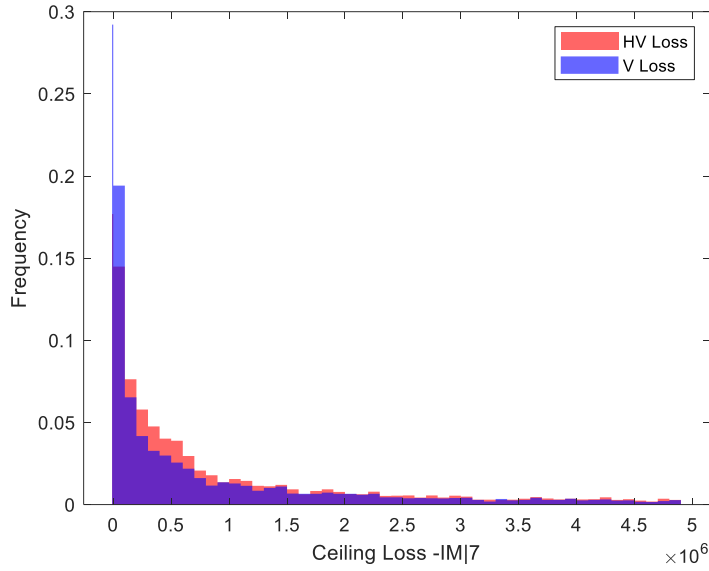**Figure 3-30: Histogram-Comparison of HV, H Loss-IM7 -CASE 2**

Figure 3-31: Histogram-Comparison of HV, V Loss-IM7 -CASE 2

Figure 3-32: Histogram-Comparison of HV, H Loss-IM7 -CASE 3
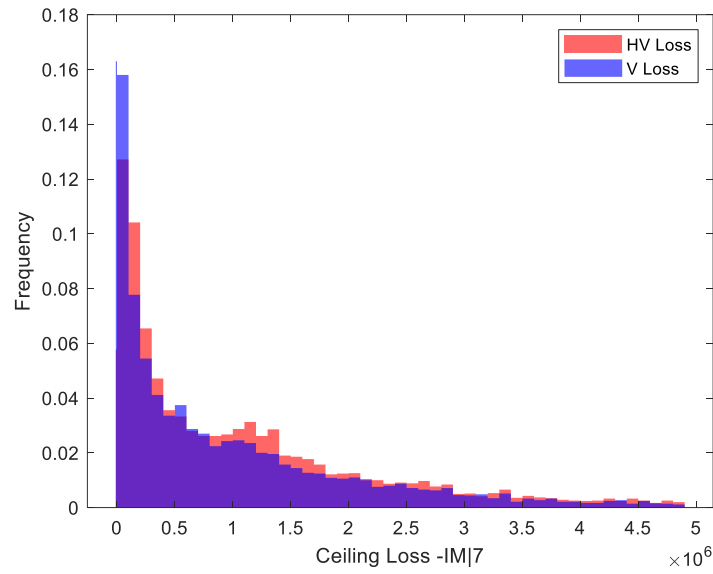
Figure 3-33: Histogram-Comparison of HV, V Loss-IM7 -CASE 3
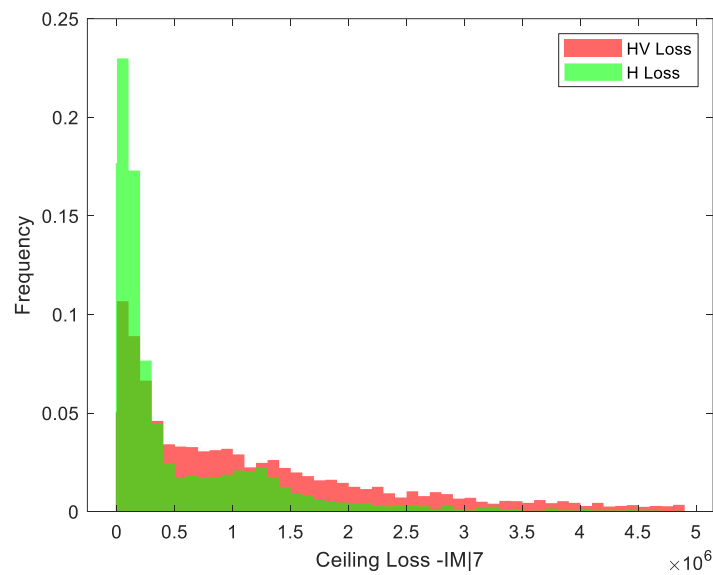
Figure 3-34: Histogram-Comparison of HV, H Loss-IM7 -CASE 4
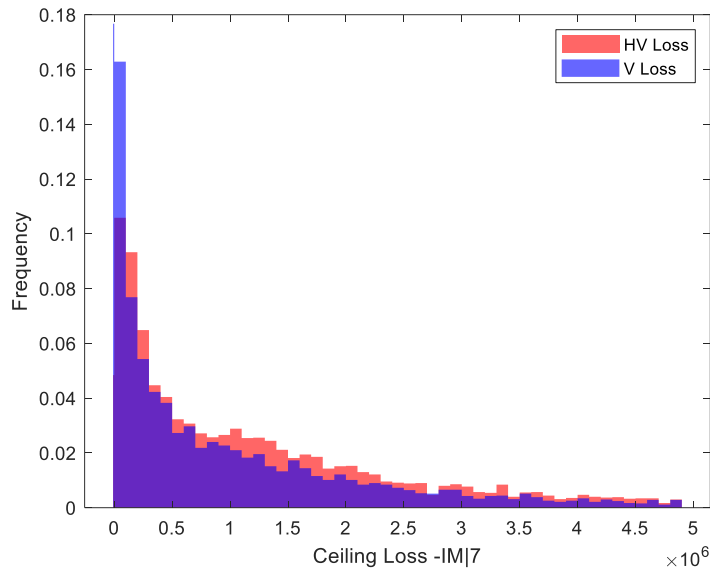
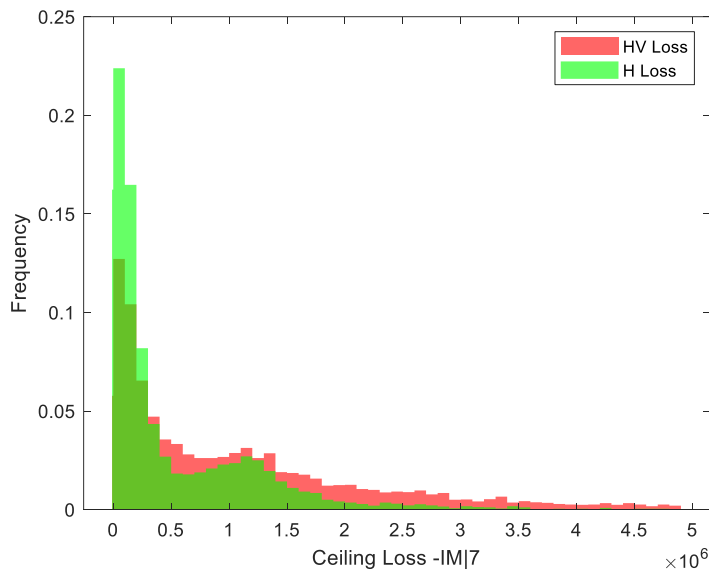**Figure 3-35: Histogram-Comparison of HV, V Loss-IM7 -CASE 4**
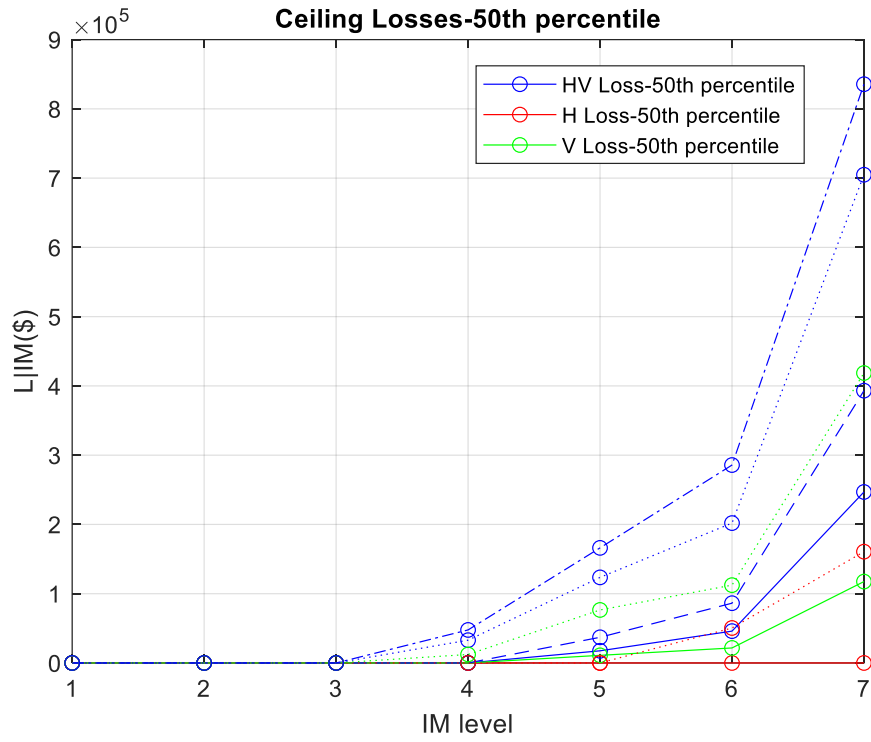
Figure 3-36: Ceiling Loss-50th percentile |IM level, with solid line being case 1, dashed line being case 2, dotted line being case 3, and dashed dotted line being case 4.
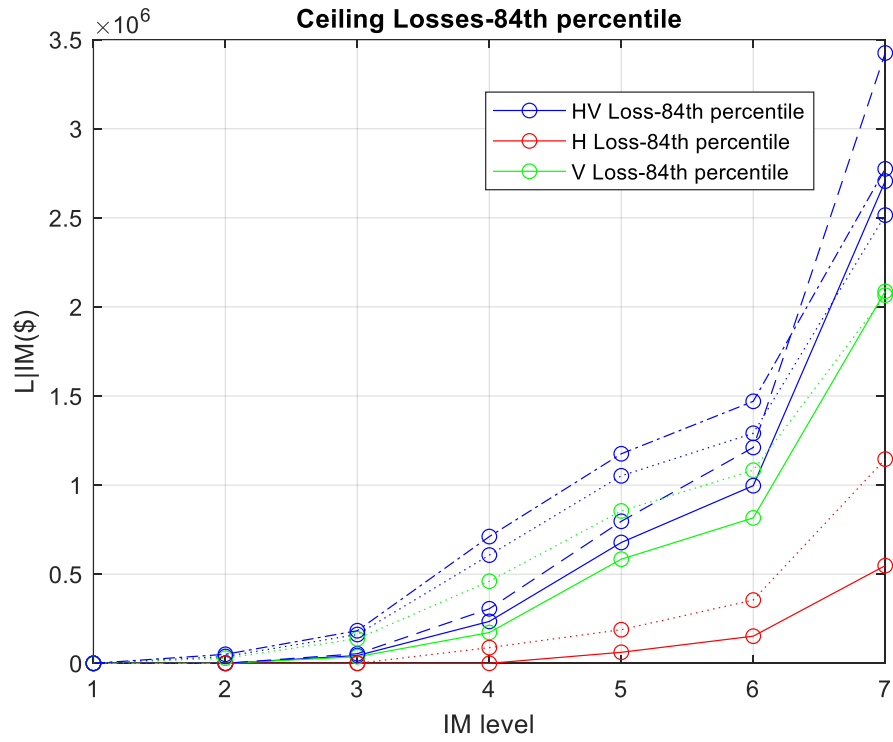
Figure 3-37: Ceiling Loss-84th percentile |IM level, with solid line being case 1, dashed line being case 2, dotted line being case 3, and dashed dotted line being case 4.

3.6 FINAL COMMENTS

The vertical component of ground motion is very rich in high frequencies and tunes with the important vertical modes of vibration of the structure. This combination results into high vertical floor accelerations and enhanced demand to the non-structural components sensitive to that vertical action. The horizontal floor acceleration is limited to lower levels due to the horizontal flexibility of the structure. In addition, the effect of the yielding at the higher IM levels will further constrain the development of high horizontal floor accelerations. Thus, neglecting the vertical component of ground motion will lead to an underestimation of the floor hazard response. By performing loss estimation of the suspended ceilings, under the combined action of the horizontal and vertical accelerations it was found that neglecting the vertical component may lead to a severe underestimation of the loss of these particular components.

4.CONCLUSIONS

This thesis discusses two illustrative cases where the vertical component of ground motion was included in the analysis. The case of the P-Δ effects shows that the inclusion of the vertical component in the analysis does not considerably change the EDP's of interest. Only some outliers were observed, with very low statistical significance. However, this finding is not at all generalizable. More structural models should be tested, along with different ground motion characteristics, and additional results might yield to materially different conclusions.

In the case of probabilistic demand of floor accelerations and loss estimation of the suspended ceilings, it was shown that the non-structural loss, especially at high IM levels, can be significant when the vertical component of ground motion is included. Thus, further research should be done in order to investigate more the effects of the vertical component in regular Seismic Risk assessment studies. Plus, more fragility criteria should be developed for other types of non-structural components that are sensitive to the vertical floor acceleration, such as fire-sprinkler system or components/contents sensitive to rocking in order to be included in the loss estimation. Moreover, the vertical acceleration response of other types of structures, such as Reinforced-Concrete structures should be addressed in future research studies.

REFERENCES

AISC. (2010). *Specification for Structural Steel Buildings (ANSI/AISC 360-10) - 2010*.

ASCE. (2016). *ASCE/SEI 7 Minimum Design Loads For Buildings and Other Structures*.

Assi, R., Dliga, M., & Yao, G. (2017). Horizontal and Vertical Seismic Acceleration Demands in Multi-Storey Buildings. *Structures Congress 2017: Business, Professional Practice, Education, Research, and Disaster Management - Selected Papers from the Structures Congress 2017*, *April 2017*, 220–231. https://doi.org/10.1061/9780784480427.019

Bazzurro, P., Kohrangi, M., Bakalis, K., & Vamvatsikos, D. (2020). *Bi-directional conditional-spectra-based record selection for horizontal and vertical ground motions. Proceedings of 17th World Conference on earthquake Engineering (17WCEE), Paper 2j-0032, Sendai, Japan, September 13-18*.

Carydis, P., Castiglioni, C., Lekkas, E., Kostaki, I., Lebesis, N., & Drei, A. (2012). The Emilia Romagna, may 2012 earthquake sequence. The influence of the vertical earthquake component and related geoscientific and engineering aspects. *Ingegneria Sismica*, *29*(2–3), 31–58.

Di Michele, F., Cantagallo, C., & Spacone, E. (2020). Effects of the vertical seismic component on seismic performance of an unreinforced masonry structures. *Bulletin of Earthquake Engineering*, *18*(4), 1635–1656. https://doi.org/10.1007/s10518-019-00765-3

Eltahawy, W., Ryan, K., Cesmeci, S., & Gordaninejad, F. (2017). *Fundamental Dynamics of 3-Dimensional Seismic Isolation*. *1508*(Abstract ID).

Fajfar, P. (2000). A Nonlinear Analysis Method for Performance-Based Seismic Design. *Earthquake Spectra*, *16*(3), 573–592. https://doi.org/10.1193/1.1586128

Fayaz, J., & Zareian, F. (2019). Reliability Analysis of Steel SMRF and SCBF Structures Considering the Vertical Component of Near-Fault Ground Motions. *Journal of Structural Engineering*, *145*(7), 04019061. https://doi.org/10.1061/(asce)st.1943-541x.0002330

Foutch, D. A., & Yun, S.-Y. (2002). Modeling of steel moment frames for seismic loads. *Journal of Constructional Steel Research*, *58*(5), 529–564. https://doi.org/https://doi.org/10.1016/S0143-974X(01)00078-5

Ghaffarzadeh, H., & Nazeri, A. (2015). The effect of the vertical excitation on horizontal response of structures. *Earthquakes and Structures*, *9*, 625–637. https://doi.org/10.12989/eas.2015.9.3.625

Gremer, N., Adam, C., Medina, R. A., & Moschen, L. (2019). Vertical peak floor accelerations of elastic moment-resisting steel frames. *Bulletin of Earthquake Engineering*, *17*(6), 3233–3254. https://doi.org/10.1007/s10518-019-00576-6

Gupta, A., & Krawinkler, H. (1999). *Seismic Demands for P Erformance Evaluation of Steel Moment Resisting Frame Structures. 132*, 141–148.

Hariri-Ardebili, M. A., & Saouma, V. E. (2016). Collapse Fragility Curves for Concrete Dams: Comprehensive Study. *Journal of Structural Engineering*, *142*(10), 04016075. https://doi.org/10.1061/(asce)st.1943-541x.0001541

Kale, Ö., & Akkar, S. (2020). A new formulation for a code-based vertical design spectrum. *Earthquake Engineering & Structural Dynamics*, *n/a*(n/a). https://doi.org/10.1002/eqe.3272

Kalkan, E., & Graizer, V. (2007). Multi-component ground motion response spectra for coupled horizontal, vertical, angular accelerations, and tilt. *ISET Journal of Earthquake Technology*, *44*.

Kazantzi, A. K., & Vamvatsikos, D. (2015). Intensity measure selection for vulnerability studies of building classes. *Earthquake Engineering & Structural Dynamics*, *44*(15), 2677–2694. https://doi.org/10.1002/eqe.2603

Kohrangi, M., Papadopoulos, A. N., Bazzurro, P., & Vamvatsikos, D. (2020). Correlation of spectral acceleration values of vertical and horizontal ground motion pairs. *Earthquake Spectra*, *36*(4), 2112–2128. https://doi.org/10.1177/8755293020919416

Korzec, A. (2016). The effect of the vertical acceleration on stability assessment of seismically loaded earth dams. *Archives of Hydroengineering and Environmental Mechanics*, *63*(2–3), 101–120. https://doi.org/10.1515/heem-2016-0007

Kwong, N. S., States, U., Survey, G., & Baker, J. W. (2020). *Selecting Three Components of Ground Motions From Selecting Three Components of Ground Motions From*. *September*.

Liberatore, D., Doglioni, C., AlShawa, O., Atzori, S., & Sorrentino, L. (2019). Effects of coseismic ground vertical motion on masonry constructions damage during the 2016 Amatrice-Norcia (Central Italy) earthquakes. *Soil Dynamics and Earthquake Engineering*, *120*(February), 423–435. https://doi.org/10.1016/j.soildyn.2019.02.015

Mckenna, F. (2011). OpenSees: A Framework for Earthquake Engineering Simulation. *Computing in Science & Engineering*, *13*, 58–66. https://doi.org/10.1109/MCSE.2011.66

Moschen, L., Medina, R. A., & Adam, C. (2016). Vertical acceleration demands on column lines of steel moment-resisting frames. *Earthquake Engineering & Structural Dynamics*, *45*(12), 2039–2060. https://doi.org/10.1002/eqe.2751

Panagiotakos, T. B., & Fardis, M. N. (2001). Deformations of reinforced concrete members at yielding and ultimate. *ACI Structural Journal*, *98*(2), 135–148. https://doi.org/10.14359/10181

Ryan, K. L., & Dao, N. D. (2016). Influence of Vertical Ground Shaking on Horizontal Response of Seismically Isolated Buildings with Friction Bearings. *Journal of Structural Engineering*, *142*(1), 04015089. https://doi.org/10.1061/(asce)st.1943-541x.0001352

Ryan, K. L., Soroushian, S., Maragakis, E. "Manos," Sato, E., Sasaki, T., & Okazaki, T. (2016). Seismic Simulation of an Integrated Ceiling-Partition Wall-Piping System at E-Defense. I: Three-Dimensional Structural Response and Base Isolation. *Journal of Structural Engineering*, *142*(2), 04015130. https://doi.org/10.1061/(asce)st.1943-541x.0001384

SeismoStruct. (2018). *SeismoSoft (2018) SeismoStruct (2018): A computer program for static and dynamic nonlinear analysis of framed structures. Available from URL www.Seismosoft.com.*

Soroushian, S., Maragakis, E. "Manos," Ryan, K. L., Sato, E., Sasaki, T., Okazaki, T., & Mosqueda, G. (2016). Seismic Simulation of an Integrated Ceiling-Partition Wall-Piping System at E-Defense. II: Evaluation of Nonstructural Damage and Fragilities. *Journal of Structural Engineering*, *142*(2), 04015131. https://doi.org/10.1061/(asce)st.1943-541x.0001385

Spears, P. W. (2004). *Parameters Influencing Seismic Structural Collapse with Emphasis on Vertical Accelerations and the Possible Related Risks for New and Existing Structures in the Central and Eastern United States.*

Vamvatsikos, D., & Fragiadakis, M. (2006). Seismic Performance Sensitivity of a 9-Story Steel Frame To Plastic Hinge Modeling Uncertainties. *First European Conference on Earthquake Engineering and Seismology*, *September*, 3–8.

Wieser, J. D. (2011). *Assessment of Floor Accelerations in Yielding Buildings.* https://scholarworks.unr.edu//handle/11714/3837

Zou, J., Li, H., & Sun, G. (2018). Analysis of influence factors of P -Δ effect considering vertical ground motion. *IOP Conference Series: Materials Science and Engineering*, *397*, 12033. https://doi.org/10.1088/1757-899X/397/1/012033

APPENDIX A. Modelling of the SDOF

The mass of the SDOF is determined as:

$$m_1^* = m_i * \Phi_{1i} \qquad\qquad (A.1)$$

Γ factor is estimated, in order to transform MDOF quantities(Q) to SDOF quantities(Q*)

$$\Gamma_1 = \frac{m_1^*}{\sum m_i * \Phi_{1i}^2} \qquad\qquad (A.2)$$

$$Q^* = \frac{Q}{\Gamma} \qquad\qquad (A.3)$$

$$D_y^* = 2 * \left(D_m^* - \frac{E_m^*}{F_y^*} \right) \qquad\qquad (A.4)$$

, and the period of the SDOF is calculated as:

$$T^* = 2\pi \sqrt{m^* \frac{D_y^*}{F_y^*}} \qquad\qquad (A.5)$$

Table A. 1 : SDOF quantities

Sdof quantities	
Γ	1.292
h_e (m)	23.74
m^* (ton)	1447.72
W (kN)	2149
F^*_y (m)	1766.9
Em^*(kNm)	336.134
D^*_y (m)	0.09352
$k0^*$ (kN/m)	18893.04
T^* (s)	1.739

In the following pages, the procedure for defining the parameters of the Opensees model is presented. In Figure A. 1, let *H* be the equivalent height of the SDOF, *he*, *P2* the vertical load of the structure, and *P1* the horizontal load applied at the top. At this point, the vertical load does not contribute to the moment equilibrium at the base since, the properties without P-Δ effects are used to define the rotational spring of the model.
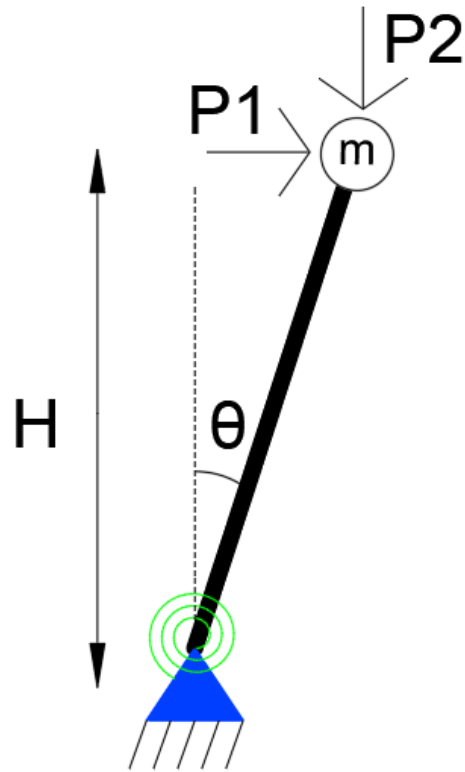
Figure A. 1: Deflected position of rigid bar-equilibrium

By taking moment equilibrium with respect to the base,

$$\sum M_{Origin} = 0$$

$$k_\theta \theta = P_1 H \qquad\qquad (A.6)$$

Let Δ, the horizontal displacement at the top,

$$\theta = \frac{\Delta}{H} \tag{A.7}$$

$$P_1 = \frac{k_\theta \Delta}{H^2} \tag{A.8}$$

The horizontal load can be written as:

$$P_1 = \left(\frac{k_\theta}{H^2}\right) * \Delta \tag{A.9}$$

, which means that the translational stiffness of the SDOF is:

$$k_{translational} = \frac{k_\theta}{H^2} \tag{A.10}$$

By replacing the yielding Force and the yielding displacement:

$$F_y = \left(\frac{k_\theta}{H^2}\right)\Delta_y \tag{A.11}$$

so, the elastic rotational stiffness of the spring is:

$$k_\theta = \frac{F_y * H^2}{\Delta_y} \tag{A.12}$$

, the yielding rotation of the spring is defined as:

$$\theta_y = \frac{\Delta_y}{H} \tag{A.13}$$

, and finally, the yielding moment:

$$M_y = F_y H \tag{A.14}$$

Table A. 2: Rotational spring parameters

Rotational spring	
k_θ (kNm/rad)	1.065×10^7
θ_y (rad)	0.0039
M_y (kNm)	4.194×10^4

The damping coefficient c, is defined as follows, where ζ is the damping ratio, ω the circular eigenfrequency and m the mass of the SDOF:

$$c = 2\zeta\omega m \qquad (A.15)$$

Table A. 3: Damper parameters

Damper	
ζ	0.05
c(kN*s/m)	522.99
L(m)	**2.37**
A(m^2)	**4.73**

In order to validate the damper and assign the proper length and area, a free vibration analysis was carried out.

$$\delta = \frac{1}{n} ln\left(\frac{x_1}{x_n}\right) \qquad (A.16)$$

$$\xi = \frac{1}{\sqrt{1 + \left(\frac{2\pi}{\xi}\right)^2}} \qquad (A.17)$$
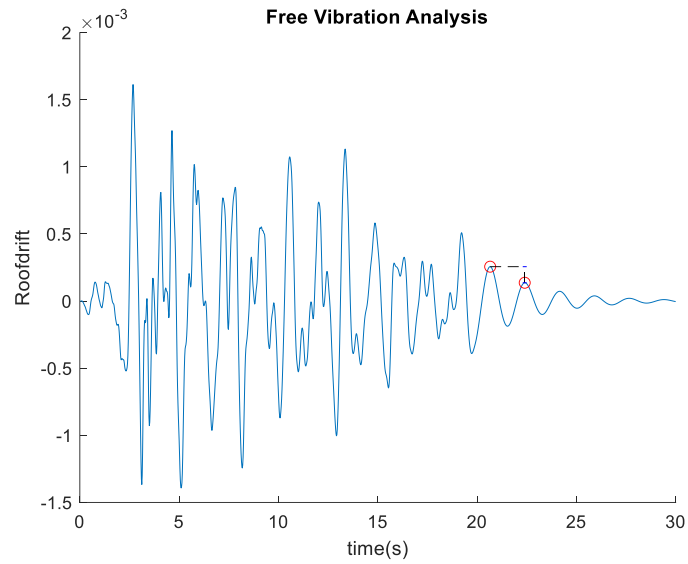
Figure A. 2: Free vibration analysis for damper validation

Table A. 4 presents the horizontal periods of the MDOF model and the corresponding mass participation factors.

Table A. 4 : MDOF model dynamic properties

Period	T(s)	$Meff_x$
1	1.61	0.85
2	0.51	0.1
3	0.27	0.03

APPENDIX B. Validation of floor-system modelling

The mass of the primary beam is turned from area to line mass.

To keep consistency between slabs across all floors, the vertical mass is assumed the same for all floors. (the mass of the typical floor, not the roof mass).

Table B. 1 : Beam properties

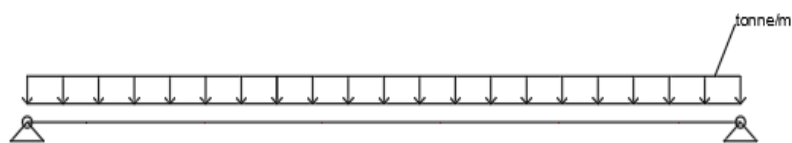| Beam section	Area mass (ton/m²)	Line mass (ton/m)	I_{comp}/I_{bare}
Primary beam	0.474	2.168	3.3
Secondary beam	0.474	0.723	3.6

Figure B. 1: Secondary beam-distributed mass

The Modal Analysis plots are visualized with the use of the Matlab software produced by Prof. Dimitrios Vamvatsikos.
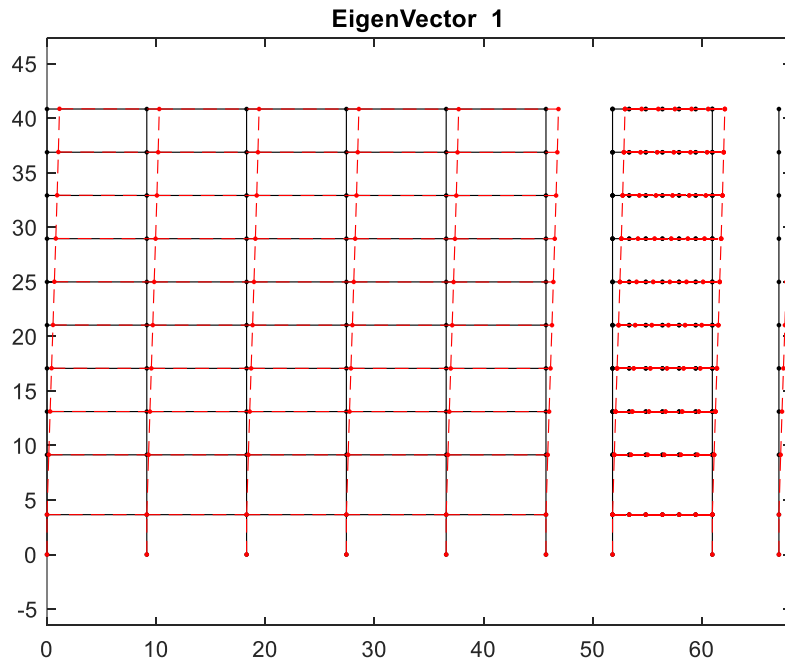
EigenVector 1

Figure B. 2: 1st horizontal mode- T=2.01s

Table B. 2: Horizontal periods of the LA9 2D model

Period	T(s)	Meff$_x$
1	2.01	0.74
2	0.76	0.11
3	0.43	0.04
6	0.28	0.03

B.1 MODEL VALIDATION

Horizontal response

A 3D representation of the LA9 building was created in SAP2000. The model is comprised by elastic elements, and its purpose is to validate, in terms of modal analysis, the OpenSees model. By setting the analysis options to Plane frame, the DOF's used for the modal analysis are, the Ux, Uz, and Ry, same as the 2D model in OpenSees. The resulting period is T=2.01s, same as the model in OpenSees. By setting the analysis options to Space Frame, all the 6 DOF's are used for the modal analysis, and the first horizontal period becomes T=2.25s. This happens because there is some mass participation of the torsional DOF in the 1st mode.
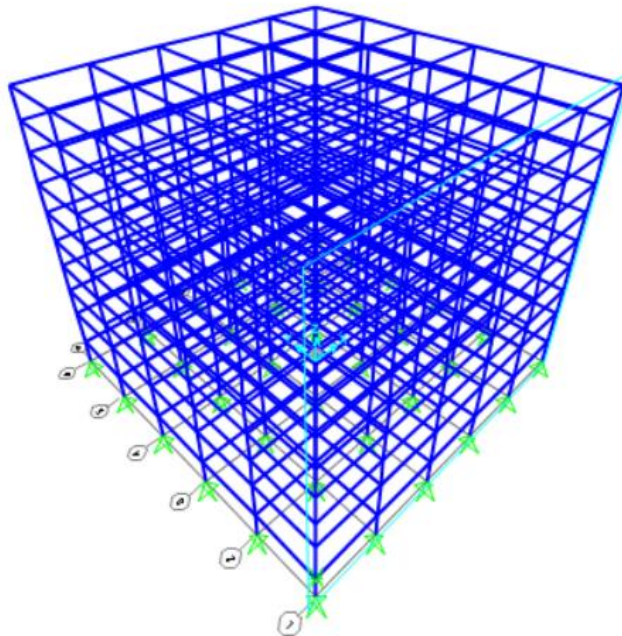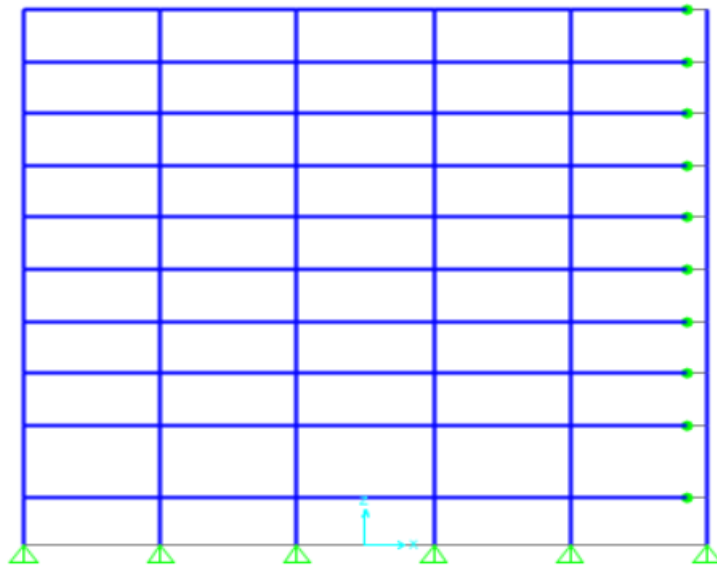

Figure B. 3: 3D model SAP2000
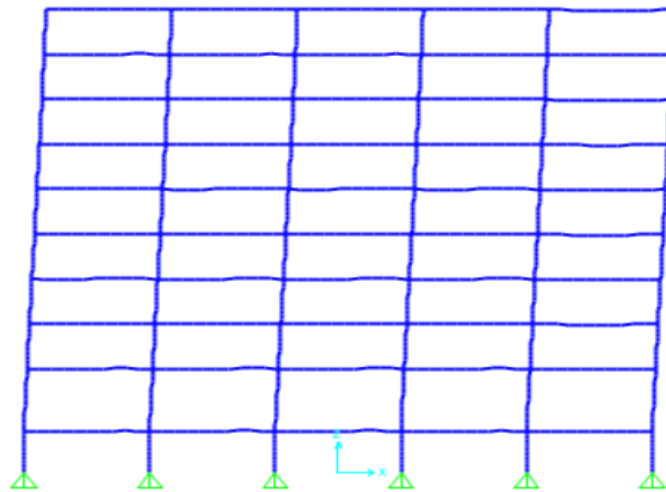
Figure B. 4: MRF SAP2000

Figure B. 5: 1st Horizontal mode SAP2000- T=2.01s

Vertical Response

Two models were created in SAP2000, in order to validate the vertical response. The 1st model has the purpose of validating the mode shape of the slab itself, while the 2nd model's purpose is to validate the mode shape of the slab and the gravity columns acting in series.

The 1st model which is presented in Figure B. 6 , is composed by 4 gravity columns, 4 primary beams and the secondary beams. The model is built with elastic elements, with the primary and secondary beams having amplified moment of Inertia, *I*, to take into account the composite action. The secondary beam to primary beam connection, as well as the primary beam to column connection is pinned. The secondary beams are discretized to smaller elements, and a line mass is applied directly to the secondary beams. The DOF's taken into account for the specific modal analysis are the *Uz*, *Rx*, *Ry*. The first vertical mode of the specific model has a period of 0.24s. This is attributed to the flexibility of the primary and secondary beams acting in series with the column axial deformation. The 2nd vertical mode of the specific model is the mode of the primary and secondary beam acting in series with a period of T=0.22s.

The 2nd model which is depicted in Figure B. 7, is composed by all the slabs of the gravity system. In that way, the gravity column is loaded by all the surrounding slabs and it's not loaded only by one slab, as it is seen in Figure 48. The SAP model has a vertical period of T=0.285s, which is less than the period coming from the OpenSees for this particular mode (T=0.32s). This happens because the SAP2000 model doesn't contain the slabs that connect the gravity system with the exterior MRF system. In that way, there is less mass on the exterior gravity columns of the specific model. With the addition of these slabs, the current period of the SAP2000 model would approach the period of the OpenSees model, which is T=0.32s.
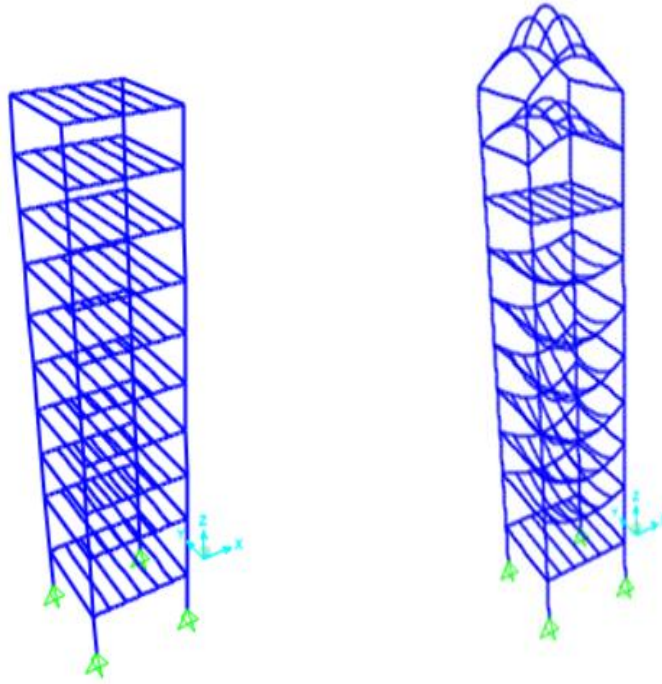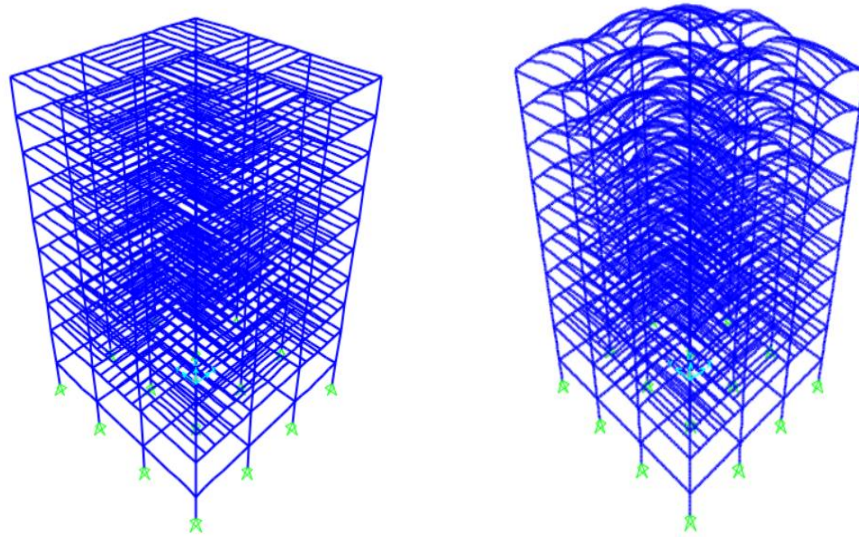
Figure B. 6: SAP2000 model- T=0.22s

Figure B. 7: SAP2000 model-slab & columns mode T=0.285s